ISSP

ACTIVITY REPORT OF SYNCHROTRON RADIATION LABORATORY

2015

Activity Report2015

TABLE OF CONTENTS

Preface Shik Shin

1. **Status of Beamline BL07LSU at the SPring-8**
2. **Status of spin- and angle-resolved photoelectron spectroscopy with laser light at LASOR**
3. **Workshops & Meetings**
4. **Seminar**
5. **Activities**

Synchrotron Radiation Experiments (Spring-8)

1) STUDY OF L-EDGE RESONANT MAGNETO-OPTIC KERR EFFECT OF A BURIED FE NANOFILM

Y. Kubota,M. Taguchi,Sh. Yamamoto,T. Someya,Y. Hirata, K. Takubo,M. Araki,
M. Fujisawa, H. Narita, K. Yamamoto, Y. Yokoyama, S. Yamamoto, H. Wadati, S. Shin,
and I. Matsuda

2) *OPERANDO* spectroNanoscopy of energy efficient devices, power generation devices and energy storage devices using 3D-Nano-ESCA and its prospects

M. Oshima, and N. Nagamura

3) OPERANDO SPECTROMICROSCOPY FOR 2D-ELECTRON TRANSISTORS FOR ENERGY-SAVING ICT

H. Fukidome

4) High-energy-resolution soft x-ray emission study of $LiCoO_2$

T. Sudayama, D. Asakura, E. Hosono, J. Miyawaki, H. Kiuchi, H. Niwa, and Y. Harada

5) CHARGE EXCITATIONS IN HIGH-TC CUPRATES STUDIED BY RESONANT INELASTIC X-RAY SCATTERING AT THE OXYGEN K-EDGE

K. Ishii, K. Sato, M. Fujita, J. Miyawaki, H. Niwa, and Y. Harada

6) VALENCE FLUCTUATION IN QUANTUM CRITICAL Yb(Al,Fe)B_4 STUDIED USING SOFT X-RAY TIME RESOLVED PHOTOEMISSION SPECTROSCOPY. II

M. Okawa, K. Akikubo, S. Yamamoto, I. Matsuda, S. Shin, S. Suzuki, S. Nakatsuji, and T. Saitoh

7) DEVELOPMENT OF PICOSECOND TIME-RESOLVED PHOTOELECTRON HOLOGRAPHY

K. Hayashi, I. Matsuda, H. Wadati, S. Yamamoto, T. Muro, T. Matsushita, and Y. Tanaka

8) EFFECT OF OXYGEN VACANCIES ON THE PHOTOEXCITED CARRIER LIFETIME ON TITANIUM DIOXIDE SURFACES

K. Ozawa, S. Yamamoto, R.-Y. Liu, K. Inoue, Ta. Higuchi, H. Sakama, K. Mase, and I. Matsuda

9) ANALYSIS OF STRUCTURES AND ELECTRONIC STATES OF [ACTIVE-SITE] IN FUNCTIONAL MATERIALS BY MICROSCOPIC HIGH-RESOLUTION TWO-DIMENSIONAL PHOTOELECTRON SPECTROSCOPY

H. Daimon, Y. Hashimoto, M. Lee, S. Fukami, D. Tsujikawa, T. Yoshida, H. Matsuda, and M. Taguchi

10) RIXS of α-Fe_2O_3 in magnetic field

J. Miyawaki, S. Suga, H. Fujiwara, H. Niwa, H. Kiuchi and Y. Harada

11) CO_2 ADSORPTION ON THE OXYGEN-MODIFIED EPITAXIAL GRAPHENE SURFACE AT NEAR AMBIENT CONDITIONS

S. Yamamoto, K. Takeuchi, R.-Y. Liu, Y. Shiozawa, T. Koitaya, T. Someya, K. Tashima, H. Fukidome, K. Mukai, S. Yoshimoto, M. Suemitsu, J. Yoshinobu, and I. Matsuda

12) ACTIVATION OF CARBON DIOXIDE ON Zn-DEPOSITED Cu SURFACES STUDIED BY AMBIENT-PRESSURE X-RAY PHOTOELECTRON SPECTROSCOPY

Y. Shiozawa, T. Koitaya, S. Yamamoto, K. Takeuchi, R.-Y. Liu, K. Mukai, S. Yoshimoto, Y. Yoshikura, I. Matsuda, and J. Yoshinobu

13) REVEALING ROOM-TEMPERATURE FERROMAGNETISM OF $ZnSnAs_2$: Mn THIN FILMS BY ATOMIC AND MAGNETIC STRUCTURE ANALYSIS BASED ON PHOTOELECTRON HOLOGRAPHY AND SITE-SELECTIVE XPS MEASUREMENTS

N. Uchitomi, M. Ogo, Y. Hashimoto, M. Lee, S. Fukami, D. Tsujikawa, T. Yoshida, H. Matsuda, M. Taguchi, and H. Daimon

14) Co 2*p*-3*d*-2*p* RESONANT X-RAY EMISSION SPECTRUM OF $LaCoO_3$ BELOW ROOM TEMPERATURE

Y. Taguchi, K. Kashiwagi M. Hamada, S. Kawamata, T. Uozumi, K. Mimura, A. Hariki J. Miyawaki, and Y. Harada

15) Improvement of *operando* cell of $LiCoO_2$ cathode for the Co 2*p* soft x-ray emission spectroscopy

D. Asakura, E. Hosono, H. Niwa, H. Kiuchi, J. Miyawaki, and Y. Harada

16) Magnetic Circular Dichroism in RIXS of weak ferromagnet α-Fe_2O_3

J. Miyawaki, S. Suga, H. Fujiwara, H. Niwa, H. Kiuchi and Y. Harada

17) ANALYSIS OF DOPANT-SITE IN BORON DOPED DIAMOND BY USING PHOTOELECTRON HOLOGRAPHY

Y. Kato

18) Monitoring the ferroelectric instability of $BaTiO_3$ by RIXS

F. Sara, M. Simon, and G. Marco

19)DEVELOPMENT OF AMBIENT PRESSURE ANGLE RESOLVED ULTRA-HIGH RESOLUTION RIXS SYSTEM

Y. Harada, J. Miyawaki, H. Niwa, H. Kiuchi, K. Yamazoe, T. Inoue, and Y. Cui

Experiments at E-labo

1) Low energy property of one-dimensional metallic surface states of Pt-induced atomic nanowires on Ge(001)

K. Yaji, and F. Komori

2) SPIN-POLARIZED SURFACE ELECTRONS IN THE NOVEL SUPERCONDUCTOR Sr_2RuO_4 REVEALED BY LASER SPIN- AND ANGLE-RESOLVED PHOTOEMISSION SPECTROSCOPY

K. Kuroda, S. Akebi, M. Nakayama, K. Yaji, H. Taniguchi, Y. Maeno, S. Nakatsuji, and T. Kondo

3) LASER SPIN-AND ANGLE-RESOLVED PHOTOEMISSION STUDY ON SPIN-ORBITAL ENTANGLED SURFACE STATES OF TOPOLOGICAL INSULATORS

K. Kuroda, K. Yaji, A. Harasawa, M. Nakayama, F. Komori, and T. Kondo

4) TESTING THE SURFACE PHOTOELECTRIC EFFECT

Y. Ishida, K. Yaji, and S. Shin

5) SPIN POLARIZATION OF 1D SURFACE STATE ON BI/INSB(001)

J. Kishi, Y. Ohtsubo, A. Harasawa, K. Yaji, F. Komori, S. Shin, and S. Kimura

Staff

Publications List

Preface

The Synchrotron Radiation Laboratory (SRL) in Institute for Solid State Physics (ISSP) has been taking part in the Synchrotron Radiation Research Organization (SRRO) of the University of Tokyo since 2005 and operating a new beamline (BL07LSU) at the SPring-8 and experimental apparatuses in soft X-ray region. The beamline has a 27m-long polarization-controlled undulator and a monochromator covering the photon energy range from 250 eV to 2 keV, which was fully opened to users since 2009. The members of solid state spectroscopy group of SRL play an essential role to promote advanced materials sciences utilizing high brilliance SR from the new undulator. In FY 2010, they have succeeded to measure time-resolved photoelectron spectroscopy of the surface photo-voltage in Si surface with the time-resolution of 30 ps by utilizing the time-structure of synchrotron radiation and an ultra-fast laser. In FYs 2011 and 2012, energy resolution of soft X-ray emission spectroscopy becomes 10,000 and the spatial resolution of the scanning photoelectron microscope (3D nano-ESCA) is better than 70 nm. In 2014, they succeeded to operate the undulator to use the circular and parallel polarization light. The first aims of BL07LSU have been achieved already. The SRL-ISSP and SRRO contribute the cutting-edge basic sciences and the applied sciences using synchrotron radiation.

June 2016

Shik Shin

Director of SRL-ISSP

1. Status of Beamline BL07LSU at SPring-8

The University-of-Tokyo high-brilliance synchrotron soft X-ray outstation beamline BL07LSU at SPring-8 has been maintained by the permanent staff members with adjuncts for user operations. A scientific aim of the beamline is to promote advanced spectroscopy for solid state and soft materials. There are currently three regular endstations: time-resolved soft X-ray spectroscopy (TR-SX spectroscopy), 3D-scanning photoelectron microscope (3D nano-ESCA) and ultrahigh resolution soft X-ray emission spectroscopy (HORNET), along with a free port station for users who bring their own experimental apparatus.

The beamline BL07LSU is equipped with a segmented cross-type undulator. In 2015, tuning of the light source was made to realize the fast polarization switching. After the machine studies in the SPring-8 storage ring, phases between electromagnetic waves, generated at the undulator segments, can be continuously controlled between $+\pi/2$ and $-\pi/2$ at 10Hz. As a consequence, the soft X-ray beam, irradiated on a sample at the end-station, can be changed between left and right circular polarizations via linear polarization at this frequency. Development of the fast polarization switching was eventually achieved.

At the beamline endstations, various scientific researches were carried out by both the laboratory staff and general users (G-type application). Below are brief introduction of recent activities at each station.

(1) Time-Resolved soft X-ray spectroscopy station (TR-SX spectroscopy)

The station is to perform time-resolved photoemission spectroscopy experiments by synchronizing the high-brilliant soft x-ray and the ultra-short laser pulses. A new type of the electron spectrometer, the two-dimensional angle-resolved time-of-flight (ARTOF) analyzer, has been used for the efficient time-resolved measurements and a low temperature manipulator (15 K) is installed for extensive experiments for users. Users have performed time-resolved photoemission measurements especially on optical functional materials, such as for solar cells and for photocatalysts. A time-resolved measurement of photoelectron diffraction was also attempted in 2015. While understanding of carrier dynamics have been one of the challenging issues in condensed matter physics, a series of the time-resolved data, accumulated by users, has captured the universal trends and the theoretical models have also been developing at the station.

(2) 3D-scanning photoelectron microscope (3D nano-ESCA)

We have developed soft X-ray scanning photoelectron emission microscopy (SPEM) with an angle-resolved electron analyzer (3D-nano-ESCA). Taking the success of operando nano-spectroscopy on organic FETs using semiconductor parameter analyzer in 2014, we have investigated pin-point electronic structure of photocatalysts for water splitting. Prof. K. Domen's group succeeded in developing novel water splitting photocatalysts $La_2Ti_5CuS_5O_7$ (LTC) and $La_2Ti_5AgS_5O_7$ (LTA) as a p-type semiconductor electrode with Sc and Ga doping [ref]. We have analyzed each photocatalyst with the size ranging from 350 nm to 1000 nm in diameter and several μm in length by 3D-nano-ESCA. It is revealed that shift of valence band spectra and core levels towards lower binding energy, suggesting successful hole doping probably into Cu 3d and Ag 4d bands by substituting Ti sites by Sc and Ga ions. [ref]

We have also attempted to analyze local electronic structure of cathode materials for Li ion batteries, that is $LiNi_{1.5}Mn_{0.5}O_4$ after charging and discharging, and found a tendency that Mn 2p core level spectra show slightly more reduced features at the edge of grain than at the plane after charging, while Ni 2p spectra show almost no difference.

Thus, operando nano-spectroscopy can provide us with useful information for improving performances of green nano-devices. However, there still remain several issues to be overcome for "more powerful" nano-spectroscopy. The most important issue is spatial resolution improvement. For nano-spectroscopy for practical nano-devices, 10 nm spatial resolution is required. The second issue is photon flux hopefully greater than 10^{10} ph/s. The third issue is ambient pressure nano-spectroscopy at several Torr. The fourth issue should be nanoARPES.

(3) Ultra high-resolution soft X-ray emission spectroscopy (HORNET)

The station is for soft X-ray emission spectroscopy measurements with ultra high-resolution ($E/\Delta E > 10^4$) and under various environmental conditions (gas, liquid and solid). In 2015, three major upgrades of the station has almost been accomplished, i.e. differential pumping system for windowless atmospheric pressure experiments (up to ~0.5 atm achieved), spectrometer rotation system for angle resolved RIXS experiments($\pm$ 45 deg. tuned), and installation of ultra-precise low slope-error post-focusing mirror to realize 1μm-level focusing of soft X-rays (total resolving power $E/\Delta E_{spectrometer}$ ~ 10000 achieved for ambient pressure and angle resolved mode). Commissioning exams of the angle resolved RIXS will be implemented in the first half of 2016 cycle and will be open to users in the second half.

The number of applications to the HORNET station is rapidly increasing. In 2015, we have accepted eight user experiments. Five among them are strongly correlated materials and the other three are battery electrode and electrolyte chemistry. We have shared our S-type long-term beamtime to trial experiments of possible users while upgrading our RIXS system for future applications.

(4) Free-port station

The station is equipped with a focusing mirror chamber, and users can connect their own experimental chambers. In 2015, the following four experiments were performed at this station: resonant soft x-ray scattering, resonant magneto-optical Kerr effects, ambient-pressure x-ray photoemission spectroscopy, and two-dimensional photoemission spectroscopy with a display-type ellipsoidal mesh analyzer. Time-resolved measurement of soft x-ray absorption spectroscopy can be made by using laser beams from the time-resolved soft x-ray spectroscopy station.

References:

[1] H. Kiuchi, T. Kondo, M. Sakurai, D. Guo, J. Nakamura, H. Niwa, J. Miyawaki, M. Kawai, M. Oshima, Y. Harada, Phys. Chem. Chem. Phys, **18**, 458-465, 2016.

[2] S. Moser, S. Fatale, P. Krüger, H. Berger, P. Bugnon, A. Magrez, H. Niwa, J. Miyawaki, Y. Harada, and M. Grioni, Phys. Rev. Lett., **115**, 9646, 2015.

[3] Sh. Yamamoto, M. Taguchi, T. Someya, Y. Kubota, S. Ito, H. Wadati, M. Fujisawa, F. Capotondi, E. Pedersoli, M. Manfredda, F. Casolari, Maya Kiskinova, J. Fujii, P. Moras, T. Nakamura, T. Kato, T. Higashide, S. Iwata, S. Yamamoto, S. Shin, and I. Matsuda, Rev. Sci. Instrum., **86**, 83901, 2015.

[4] Yi-Sheng Liu, Per-Anders Glans, Cheng-Hao Chuang, Mukes Kapilashramic, Jinghua Guo, Journal of Electron Spectroscopy and Related Phenomena, **200**, 282-292, 2015.

[5] R. Yukawa, K. Ozawa, S. Yamamoto, R.-Y. Liu, and I. Matsuda, Surf. Sci., **641**, 224-230, 2015.

[6] N. Nagamura, Y. Kitada, J. Tsurumi, H. Matsui, K. Horiba, I. Honma, J. Takeya and M. Oshima, Appl. Phys. Lett., **106**, 251604, 2015.

[7] 吹留　博一, 表面科学, **36** (6), 303-308, 2015.

[8] K. Kurita, D. Sekiba, I. Harayama, K. Chito, Y. Harada, H. Kiuchi, M. Oshima, S. Takagi, M. Matsuo, R. Sato, K. Aoki, S. Orimo, J. Phys. Soc. Jpn., **84**, 043201, 2015.

[9] T. Tsuyama, T. Matsuda, S. Chakraverty, J. Okamoto, E. Ikenaga, A. Tanaka, T. Mizokawa, H. Y. Hwang, Y. Tokura, and H. Wadati, Phys. Rev. B, **91**, 115101, 2015.

[10] J. Sellberg, T. McQueen, H. Laksmono, S. Schreck, M Beye, D. DePonte, B. O'Kennedy, D. Nordlund, R. Sierra, D. Schlesinger, T. Tokushima, S. Eckert, V. Segtnan, H. Ogasawara, K.

Kubicek, S. Techert, U. Bergmann, G. Dakovski, W. Schlotter, Y. Harada, I. Zhovtobriukh, M. Bogan, P. Wernet, A. Föhlisch, L. Pettersson and A. Nilsson, J. Chem. Phys., **142**, 044505, 2015.
[11] M.M. van Schooneveld and S. DeBeer, J. Electron Spectrosc. Relat. Phenom., **198**, 31, 2015.
[12] D. Asakura, E. Hosono, H. Niwa, H. Kiuchi, J. Miyawaki, Y. Nanba, M. Okubo, H. Matsuda, H.S. Zhou, M. Oshima, and Y. Harada, Electrochem. Commun., **50**, 93, 2015.

2. Status of spin- and angle-resolved photoelectron spectroscopy with laser light at Laser and Synchrotron Research Laboratory

Spin- and angle-resolved photoelectron spectroscopy (SARPES) is a powerful technique to investigate the spin-dependent electronic states in solids. We developed a SARPES apparatus with a vacuum-ultraviolet laser at Laser and Synchrotron Research Laboratory in the Institute for Solid State Physics, named LOBSTER (Laser-Optics-Based Spin-vecTor Experimental Research) machine. The LOBSTER machine is utilized to obtain precise information on spin-dependent electronic structures near the Fermi level in solids. We started a project to construct the LOBSTER machine from FY 2014 and joint researches at this station have started from FY 2015.

Figure 1 represents an overview of the LOBSTER machine. The apparatus consists of an analysis chamber, a sample-bank chamber connected to a load-lock chamber, and a molecular beam epitaxy (MBE) chamber, which are kept in an ultra-high vacuum (UHV) environment and are connected with each other via UHV gate valves. The hemispherical electron analyzer is a custom-made ScientaOmicron DA30-L, modified to attach the very-low-energy-electron-diffraction type spin detectors. The electrons are excited by 6.994-eV photons, yielded by 6th harmonic of a Nd:YVO_4 quasi-continuous wave laser with repetition rate of 120 MHz. A helium discharge lamp (VG Scienta, VUV5000) is also available as a photon source. At the MBE chamber, samples can be heated by a direct current heating or electron bombardment. The surface evaluating and preparing instruments, such as evaporators, low energy electron diffraction, reflection high energy electron diffraction, sputter-gun and quartz microbalance, can be installed. At the carousel chamber, 16 samples can be stocked in the UHV environment.

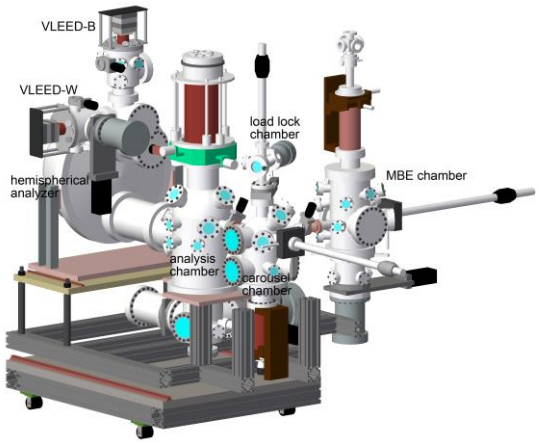

Fig. 1. Overview of the LOBSTER machine at LASOR [1].

Figure 2 shows a Fermi edge taken from a gold (Au) thick film recorded with the SARPES mode. The sample temperature was set to 9 K. The spectrum was taken with the analyzer pass energy of 2 eV. The sizes of an entrance slit and an exit aperture are set to 0.2 mm and 0.2 × 0.5 mm^2,

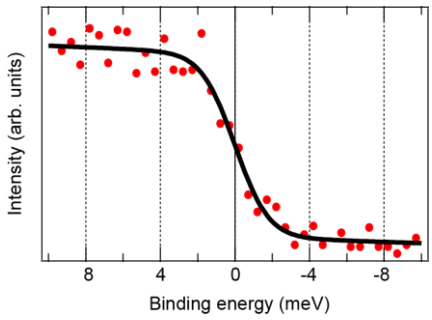

Fig. 2 The Fermi edge taken from a Au thick film recorded in SARPES mode [1].

respectively. The spectrum was fitted with the Fermi distribution function. From the fitting, the energy resolution was estimated to be 1.7 meV for the SARPES mode.

We performed laser-ARPES and laser-SARPES measurements of the Bi(111) surface. Figure 3(a) shows a Fermi-surface mapping recorded with the ARPES mode. The energy and angular resolutions of the instrument were set to 1.5 meV and 0.1°, respectively. The acquisition time for the Fermi surface image is 3 min. We found a hexagonal Fermi surface around $\bar{\Gamma}$ and a part of six Fermi surfaces elongated in the $\bar{\Gamma}\bar{M}$ direction, which originate from surface states. Figure 3(b) shows spin-resolved photoelectron spectra taken at a selected angle shown in Fig. 3(a). The spin detector is arranged to be sensitive to the spin polarization of P_y on the sample axis, which corresponds to the spin polarization direction expected by the ordinary Rashba effect. In the SARPES measurements, the energy and angular resolutions were set to 7 meV and 0.7°, respectively. The acquisition time of a pair of spectra is 15 min. We clearly observed the spin polarization of the surface states arising from the Rashba effect. From this demonstration, it is clear that the new spectrometer can provide high-resolution spin-resolved spectra in a very short time. The error-bars of the spin polarization are as small as 3 %, indicating the high accuracy of the new spectrometer.

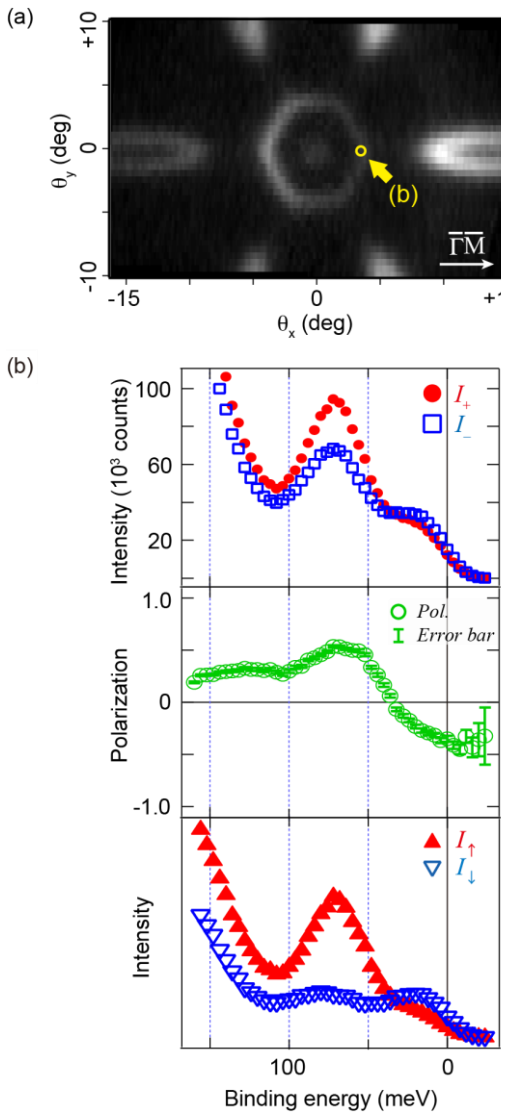

Fig. 3 (a) Constant energy ARPES intensity map at the Fermi level of the Bi(111) surface. (b) SARPES spectra measured at a selected *k* point shown by a circle in (a). The upper panel represents raw spectra. Calculated spin polarization is exhibited in the middle panel. The bottom panel represents the spin-resolved spectra [2].

References

[1] K. Yaji, A. Harasawa, K. Kuroda, S. Toyohisa, M. Nakayama, Y. Ishida, A. Fukushima, S. Watanabe, C.-T. Chen, F. Komori and S. Shin, Rev. Sci. Instrum. **87**, 053111 (2016).

[2] K. Yaji, Hyomenkagaku 37, 19 (2016).

3. Workshops & Meetings

A report of the commemorative lecture meeting, celebrating 10th anniversary of Synchrotron Radiation Research Organization in the University of Tokyo

Iwao Matsuda

Synchrotron Radiation Research Organization, the University of Tokyo

Institute for Solid State Physics, the University of Tokyo

A commemorative lecture meeting was held at Koshiba-hall (Hongo campus, the University of Tokoyo) on November 13, 2015, to celebrate 10th anniversary of Synchrotron Radiation Research Organization in the University of Tokyo. Participants of 123 people (including 78 from the University of Tokyo) were gathered and the meeting was great success. The program was organized with the anniversary event and the commemorative lectures.

In the anniversary event, addresses were given by Prof. Yoshiyuki Amemiya (Director of Synchrotron Radiation Research Organization, the University of Tokyo), Prof. Hitoshi Takigawa (Director of Institute of Solid State Physics, the University of Tokyo), and Prof. Tetsu Akiyama (Director of Institute of Molecular and Cellular Biosciences, the University of Tokyo). Then, greeting words were honorably presented by Prof. Kazuo Hotate (Vice-president of the University of Tokyo) and Dr. Yoshiharu Doi (President of Japan Synchrotron Radiation Research Institute).

Three commemorative lectures were delivered by three outstanding researchers, Dr. Anders Nilsson (Professor of SLAC, Stanford University, Stockholm University), Dr. Yoshiki Higuchi (Professor of University of Hyogo) and Dr. Tetsuya Ishikawa (President of RIKEN SPring-8 Center). Then, recent research activities in Synchrotron Radiation Research Organization were described by the two division leaders, Prof. Shik Shin and Prof. Chikashi Toyoshima.

At the end, closing address was given by Prof. Masaharu Oshima (Former Director of Synchrotron Radiation Research Organization, the University of Tokyo).

Figure 1 The commemorative photo

(at the front from left) Prof. Anders Nilsson, Prof. Yoshiki Higuchi、Dr. Tetsuya Ishikawa, Dr. Yoshiharu Doi, Vice-President Kazuo Hotate, Vice-President Ken Furuya, Prof. Hitoshi Takigawa, and Prof. Tetsu Akiyama.

(at the rear from left) Prof. Shik Shin, Prof. Yoshiyuki Amemiya, Prof. Masaharu Oshima, and Prof. Chikashi Toyoshima

Figure 2 A photo of the guests, the lecturers, and the participants

The 29th Annual Meeting/Joint Symposium of the Japanese Society of Synchrotron Radiation Research

Iwao Matsuda, Shik Shin

The Institute for Solid State Physics, the University of Tokyo, Japan

Synchrotron Radiation Research Organization, the University of Tokyo, Japan

The 29th Annual meeting/joint symposium of the Japanese Society for Synchrotron Radiation Research was held at Kashiwa campus in the University of Tokyo from January 9 to 11 in 2016. The synchrotron radiation laboratory contributed as the main members of the executive committee. Prof. Shik Shin and Prof. Iwao Matsuda served as the chairman and the vice-chairman, respectively. The meeting/symposium was held as cooperative works with the program committee (Chairman: Prof. Atsushi Fujimori, Vice-chairman: Takahisa Arima) and the organizing committee (Chairman: Dr. Yuya Shinohara). During the period, there were 703 participants, 343 presentations (oral and poster), and 59 company exhibitions. At the banquet, there are 372 attendants, including 49 students. The participants enjoyed the meeting/symposium and learned much from the excellent presentations and discussion. The details were reported as an article in the domestic journal published by the Japanese Society for Synchrotron Radiation Research (放射光 29 (2), 90 (2016)).

Fig.1 Entrance of the hall and posters

Fig.2 Oral presentation

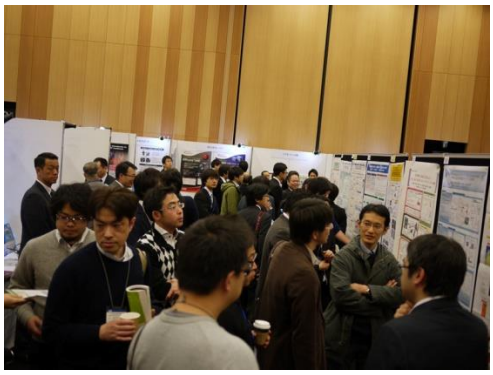

Fig.3 Poster session

Fig.4 The honor lecture by Prof. M. Oshima

Fig.5 The honor lecture by Prof. T. Irifune

Fig.6 The poster

Fig.7 Address by President Makoto Gonokami of the University of Tokyo at the banquet.

Fig.8 The banquet

ISSP workshop " Status of SPring-8 BL07LSU
-Integration of x-ray spectroscopy and diffraction-"

Date: 2016/3/1(Tue)

Place: Lecture Room (A632), 6th Floor, ISSP, the University of Tokyo

Synchrotron radiation laboratory has a Harima branch to maintain and develop a high-brilliance soft X-ray beamline BL07LSU at SPring-8. There we are performing time-resolved, spatial-resolved and energy-resolved soft X-ray spectroscopy to study electronic states and their dynamics of new materials. In this workshop, recent research activities at our beamline were reported and we discussed our new experimental techniques which integrate x-ray spectroscopy and diffraction. The speakers talked about their recent results from each end station (time-resolved spectroscopy, 3D nano-ESCA, emission spectroscopy, and so on). There were two invited talks; one is about synthesizing novel superconductors and the advantage of using synchrotron x-rays for finding new materials, and the other is about coherent x-ray scattering using synchrotron x-rays and x-ray free electron lasers.
There were a lot of discussions for each talk, and we successfully started to obtain a clear vision about our future experimental techniques combining x-ray spectroscopy and diffraction. We also encouraged the young generation in this research field by awarding the best poster prize to one graduate student.

Program

10:00- **Opening Address** Hiroshi Kondo (Keio University, VSX Users' Organization)

10:05- **Guest Address** Ryotaro Tanaka (JASRI)

10:10- **Introduction** Shik Shin (ISSP, the University of Tokyo)

10:20- **Status of developing the cross-undulator light source at SPring-8 BL07LSU**
Iwao Matsuda (ISSP, the University of Tokyo)

10:45- **Exploration of Novel Superconductors using Arsenic Chemistry**
Minoru Nohara (Okayama University)

11:25- **Poster short Presentation**

11:50- **lunch**

13:00- **Poster session**

14:00- **Operando nano-spectroscopy for energy efficient, power generation and energy storage devices**
Masaharu Oshima (SRRO, the University of Tokyo)

14:30- **Development of high resolution / angle resolved / ambient pressure soft X-ray emission spectroscopy system**
Yoshihisa Harada (ISSP, the University of Tokyo)

15:00- **Studying spin dynamics by using polarization of x-rays**
Hiroki Wadati (ISSP, the University of Tokyo)

15:30- **Live cell nano-imaging using X-ray free-electron laser**
Yoshinori Nishino (Research Institute for Electronic Science, Hokkaido University)

16:10- **Coffee Break**

16:30- **Development of picosecond time-resolved photoelectron holography using VO_2 thin films**
Koichi Hayashi (Nagoya Institute of Technology)

16:50- **Surface State Analysis on GaN-based Transistor**
Yasunori Tateno (Sumitomo Electric Industries Ltd)

17:10- **Electric Structure of CrO_2 Probed by High-Resolution Soft-X-ray Resonant Inelastic X-ray Scattering in Magnetic Field**
Hidenori Fujiwara (Grad. Sch. of Eng. Sci. Osaka University)

17:30- **Analysis of Structures and Electronic States of [Active-site] in Functional Materials by Microscopic High-resolution Two-Dimensional Photoelectron Spectroscopy**
Munetaka Taguchi (Nara Institute of Science and Technology)

17:50- **Operando observation of the activation and hydrogenation processes of CO_2 on Cu based model catalysts using ambient pressure photoelectron spectroscopy at the freeport of SPring-8 BL07LSU**
Jun Yoshinobu (ISSP, the University of Tokyo)

18:10- **Closing address** Yoshiyuki Amemiya (The University of Tokyo)

4. Seminar

(ISSP Lectures by Visiting Professors)
Date: April 16, 2015
Title: Observation of quadrupole moment ordering with resonant x-ray diffraction
Speaker: Dr. Yoshikazu Tanaka (RIKEN)

(ISSP Colloquium)
Date: May 7, 2015
Title: Soft X-ray emission spectroscopy: trends and recent topics in SPring-8
Speaker: Dr. Yoshihisa Harada (ISSP, the University of Tokyo)

Date: May 7, 2015
Title: Resonant Inelastic X-ray Scattering research of strongly correlated electron systems at NSRRC -Sr_3NiIrO_6 and Bi2212-
Speaker: Dr. Jun Okamoto (National Synchrotron Radiation Research Center)

Date: May 11, 2015
Title: Spin-resolved simultaneous 2D-ARPES with very high spin detection efficiency by combining a PEEM, momentum microscope and 2D imaging spin filter
Speaker: Dr. Shigemasa Suga (Max-Planck-Institute of Microstructure Physics, Halle, Germany. Institute of Sci. & Ind. Research, Osaka University, Japan)

(LASOR Seminar)
Date: June 9, 2015
Title: Optical excitation of topological magnetic orders
Speaker: Dr. Naoki Ogawa (RIKEN CEMS)

Date: July 22, 2015
Title: Understanding biological processes through 3D structures of proteins-molecular mechanisms of tumor suppression and neural circuit formation
Speaker: Dr. Shuya Fukai (SRRO, the University of Tokyo)

Date: September 1, 2015
Title: Fundamental Study on the Functional Thiolate Self-Assembled Monolayers: its Photoexcitation and Multi-Function Attachment
Speaker: Dr. Hiroyuki S. Kato (Graduate School of Science, Osaka University)

Date: November 11, 2015
Title: Prediction of an arc-tunable Weyl Fermion metallic state in MoxW1-xTe2
Speaker: Dr. Tay-Rong Chang (National Tsing Hua University)

Date: November 25, 2015
Title: Silicene, germanene and stanene: novel synthetic 2D electronic materials beyond graphene
Speaker: Dr. Guy Le Lay (Aix-Marseille University)

Date: December 8, 2015
Title: Quantum anomalous Hall effect in magnetic topological insulators
Speaker: Dr. Ke He (Tsinghua University)

Date: March 8, 2016
Title: Elucidation of the folding movement of proteins by the high-speed single molecule fluorescence spectroscopy
Speaker: Dr. Satoshi Takahashi (Tohoku University)

Date: March 18, 2016
Title: Determining the valence of Mn4Ca clusters in the active site of photosystem II in photosynthesis
Speaker: Dr. Yasufumi Umena (Contract associate professor, Okayama University)

STUDY OF L-EDGE RESONANT MAGNETO-OPTIC KERR EFFECT OF A BURIED FE NANOFILM

Y. Kubota,[1] M. Taguchi,[2] Sh. Yamamoto,[1] T. Someya,[1] Y. Hirata,[1] K. Takubo,[1] M. Araki,[1] M. Fujisawa,[1] H. Narita,[1] K. Yamamoto,[1] Y. Yokoyama,[1] S. Yamamoto,[1] H. Wadati,[1] S. Shin,[1] and I. Matsuda[1]

[1]*Institute for Solid State Physics, The University of Tokyo, Kashiwa-no-ha, Kashiwa, Chiba 277-8581, Japan*

[2]*RIKEN SPring-8 Center, Sayo, Hyogo 679-5148, Japan*

Introduction

Magnetism has been one of the central issues in condensed matter physics and the magnetic information has been measured experimentally by means of the magneto-optical effects, such as magneto-optical Kerr effect (MOKE). In the MOKE measurement, rotation of the light polarization plane is measured before and after refection at a sample surface. Change of the polarization angle is defined as the Kerr rotation angle (θ_K) that depends on magnetization of a sample. The θ_K value typically ranges < 1 degree for a bulk crystal of magnetic transition metal, such as Fe, Co and Ni, when it is measured with visible light. On the other hand, it has been reported recently that the θ_K becomes significantly large in the ultraviolet ~ X-ray region when a probing photon energy is tuned at the absorption edge of the element atoms that compose a sample. The phenomenon has been called the resonant MOKE (RMOKE) and it has allowed us to evaluate magnetic properties of a material with element-selectivity and resonant enhancement. In a case of RMOKE for a Fe film, the experimental θ_K value reaches 10 degree at the L_3 and L_2 photon energy region. On the other hand, research of the first principle calculation reported that θ_K is about 50 degree when photon energy is at the Fe L_2-edge for the bulk Fe metal. There still remains discrepancy of the θ_K values between experiment and theory, which requires their systematic comparisons of the RMOKE spectra for proper understandings of the magneto-optical phenomena.

In the present research, we examined L-edge RMOKE of the buried Fe nanofilm by comparing θ_K spectra obtained by the measurement and by calculations with two-types of theoretical models: classical electromagnetic and quantum-mechanics.

Experimental method

Figure 1 (a) shows a schematic drawing of heterostructure of the Ta/Cu/Fe/MgO sample. A 30-nm-thick Fe film was grown on the MgO(001) substrate and it was capped with Ta (2 nm thick) and Cu (2 nm thick) layers to prevent the Fe layer from oxidization. The buried Fe nanofilm has an in-plane easy direction of magnetization. Measurement of RMOKE was made at the SPring-8 BL07LSU beamline with geometry of longitudinal MOKE (L-MOKE), as shown in Fig.1 (b). The *s*-polarized light was incident onto the sample with incident angle (θ_i) of about 80 degree with respect to the surface normal. Magnetic field (B) of +/- 0.3 T was applied along in-plane direction of the sample surface, which is large enough to saturate the Fe magnetization. A θ_K value was measured by the rotating-analyzer ellipsometry (RAE) method. The RAE unit was composed of a multi-mirror and a micro-channel plate (MCP) as shown in Fig. 1(b). Details of the measurement technique can be found elsewhere. In brief, θ_K can be determined from difference of the ellipsometry curves taken at the opposite magnetic field: $2\theta_K = \theta\,(+B) - \theta\,(-B)$, as shown in Fig. 1 (c)

Results and discussion

Figure 2 (a) shows the θ_K spectrum of the buried Fe nanofilm taken at Fe $L_{2,3}$-edges. It shows two peaks with negative and positive θ_K values that are 7.1 and -18.2 degrees and correspond to the L_2 and L_3 absorption edges, respectively. In Fig. 2 (b), a curve of the θ_K spectral simulation, based on classical electromagnetic theory with the empirical optical constants. Comparing with the measured value in Fig.2 (a), one finds that the two results of the experiment and the calculation match with each other overall, reproducing the sign inversion of θ_K between the L_2 and L_3 absorption edges. Results of this quantum-mechanical spectral calculation based on the configuration interaction (CI) model in Fig. 2 (c) show good agreement with the experimental θ_K spectral feature at pre-edge of the Fe L_3-edge (Fig.2(a)). In contrast to the phenomenological calculation, the dip-like structure at 707 eV is reproduced, which is likely derived from the quantum-mechanical effect. Near the L_2-edge, however, the CI model calculation indicates large θ_K = 48 degree. Moreover, its simulated spectrum does not show the sign inversion in Fe L-edge energy region, which contradict to the experimental result.

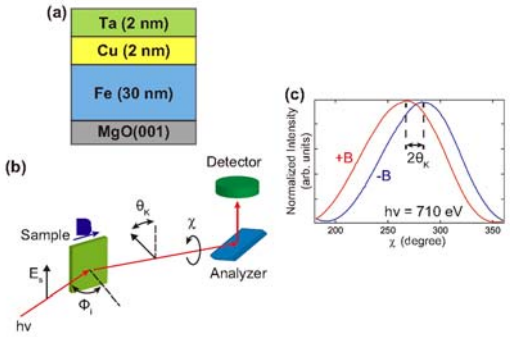

FIG. 1: (a) A schematic drawing of the 30-nm-thick Fe film on the MgO(001) substrate. Ta (2 nm) and Cu (2 nm) are capping layers. (b) A set up of L-MOKE measurement with RAE. RAE composed by a multi-mirror and a MCP. (c) Typical results of the intensity variation with rotation angle, χ, taken at $h\nu = 710$ eV. The red and blue solid lines represent the spectra obtained when the magnetic field were +0.3 T ($+B$) and 0.3 T ($-B$), respectively. The Kerr rotation angle can be determined from $2\theta_K = \theta(+B) - \theta(-B)$.

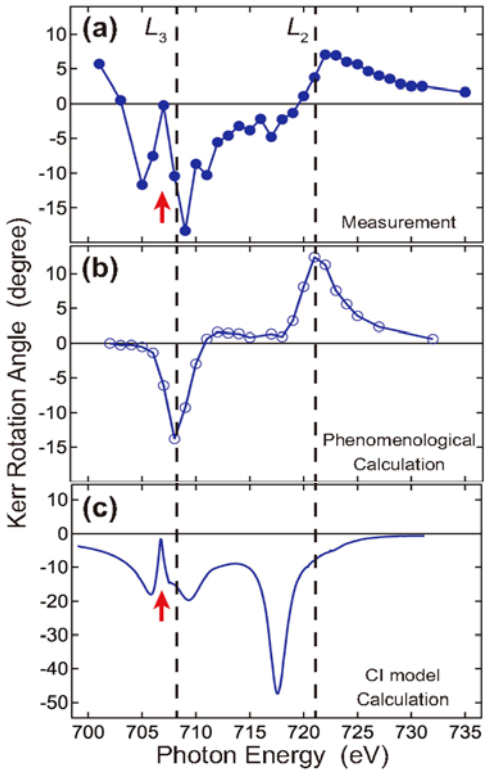

FIG. 2: θ_K spectra of the buried Fe nanofilm at Fe $L_{2,3}$-edges obtained by the measurement (a), the classic electromagnetic calculation with the empirical optical constants (b) and the quantum-mechanical calculation with the CI model (c). Two dashed lines represent L_2 and L_3 adsorption edges. The arrows represent the dip-like structure near L_3-edge in (a) and (c). The error bar of experimental data is smaller than the size of filled circle.

Operando spectroNanoscopy of energy efficient devices, power generation devices and energy storage devices using 3D-Nano-ESCA and its prospects

[1]Masaharu Oshima and [2]Naoka Nagamura
[1]*Synchrotron Radiation Research Organization, The University of Tokyo, Tokyo, Japan,*
[2]*National Institute for Materials Science (NIMS), Tsukuba, Ibaraki, Japan*

In order to investigate pin-point electronic structure in green nano-devices such as energy efficient devices like ReRAM and graphene FET, power generation devices like fuel cells and photocatalysts for hydrogen generation and energy storage devices like Li/Na ion batteries during device operation, we have developed soft X-ray scanning photoelectron emission microscopy (SPEM) with an angle-resolved electron analyzer (3D-nano-EASCA). The spatial resolution was determined to be 70 nm [1]. Furthermore, we modified 3D-nano-ESCA so that different voltages can be independently applied to five electrodes for gate, source, drain and ground in a sample holder connected to a semiconductor parameter analyzer.

The first example for energy efficient devices is organic FET which has attracted great attention because of their unique properties such as light weight, flexible electronics and low cost. Prof. J. Takeya's group succeeded in developing good performance OFETs using single-crystalline C10-DNBDT-NW films on SiO_2 (200 nm)/Si substrates [2]. In this study, OFETs for *operando* nano-spectroscopy were fabricated using ultrathin (3ML or 12 nm) single-crystalline C10-DNBDT-NW films on SiO_2 (200 nm)/Si substrates, with a backgate electrode and top source/drain Au electrodes. C 1*s* line profiles under biasing at the backgate and drain electrodes were measured. Figure 1 shows schematic of SPEM measurements, (b) Sample holder with five individual electrodes, optical microscope image of OFET, and Au 4*f* SPEM of OFET. As shown in Fig. 2, this ultrathin OFET exhibits good electrical properties. *Operando* measurements of line profiles of C 1*s* binding energy across the OFET channel from drain to source, and gate bias voltage dependence of C 1s binding energy and drain current are shown in Fig. 3, suggesting that drain current proportional to hole concentration in the channel generated by the back gate biasing is well correlated by the simple Boltzmann distribution with the chemical potential [3]. Furthermore, potential profiles in the channel from source to drain are in good agreement with potential profiles calculated by gradual channel approximation (GCA) [4].

As for power generation devices, we have investigated pin-point electronic structure of photocatalysts for water splitting. Prof. K. Domen's group succeeded in developing novel water splitting photocatalysts $La_2Ti_5CuS_5O_7$ (LTC) and $La_2Ti_5AgS_5O_7$ (LTA) as a *p*-type semiconductor electrode with Sc and Ga doping [5]. We have analysed each photocatalyst with the size ranging from 350 nm to 1000 nm in diameter and several μm in length (Fig. 4) by 3D-nano-ESCA. It is revealed that shift of valence band spectra and core levels towards lower binding energy, suggesting successful hole doping probably into Cu 3*d* and Ag 4*d* bands by substituting Ti sites by Sc and Ga ions. [6]

We have also attempted to analyze local electronic structure of cathode materials for Li ion batteries, that is $LiNi_{1.5}Mn_{0.5}O_4$ after charging and discharging, and found a tendency that Mn 2*p* core level spectra show slightly more reduced features at the edge of grain than at the plane after charging, while Ni 2*p* spectra show almost no difference.

Thus, *operando* spectroNanoscopy can provide us with useful information for improving performances of green nano-devices. However, there still remain several issues to be overcome for "more powerful" spectroNanoscopy. The most important issue is spatial resolution improvement. For spectroNanoscopy for practical nanodevices, 10 nm spatial resolution is required. The second issue is photon flux hopefully greater than 10^{10} ph/s. The

third issue is ambient pressure spectroNanoscopy at several Torr. The fourth issue should be nanoARPES.

We'd like to thank H. Matsui, J. Tsurumi, J. Takeya, E. Sakai, T. Hisatomi, K. Domen, D. Asakura, and E. Hosono for their collaborations.

REFERENCES:

[1] K. Horiba *et al.*, Rev. Sci. Instrum. **82**, 113701 (2011).
[2] J. Soeda *et al.*, Applied Physics Express **6**, 076503 (2013).
[3] N. Nagamura *et al.*, Appl. Phys. Lett. 106, 251604 (2015).
[4] N. Nagamura *et al.*, to be submitted.
[5] J-Y. Li *et al.*, Energy and Environmental Science DOI: 10.1039/c4ee00091a, (2014).
[6] E. Sakai *et al.*, to be submitted.

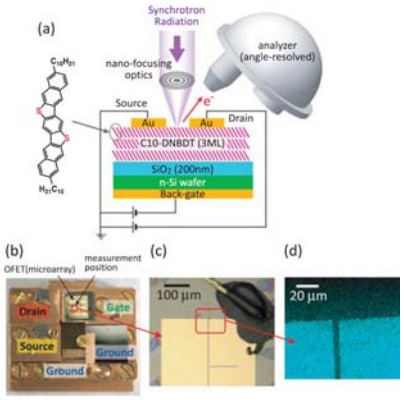

Fig. 1. (a) Schematic of SPEM measurements, (b) sample holder, (c) optical microscope image of OFET, (d) Au 4*f* SPEM of OFET.

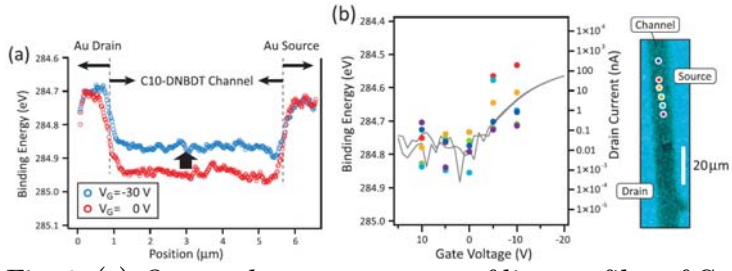

Fig. 3. (a) *Operando* measurements of line profiles of C 1s binding energy across the OFET channel from drain to source, (b) gate bias voltage dependence of C 1s binding energy and drain current.

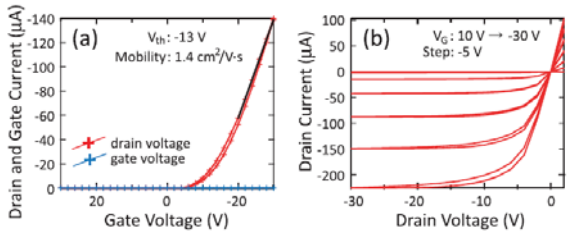

Fig. 2. (a) Typical drain and gate current as a function of gate voltage for OFET and (b) typical drain current as a function of drain voltage at different gate voltage.

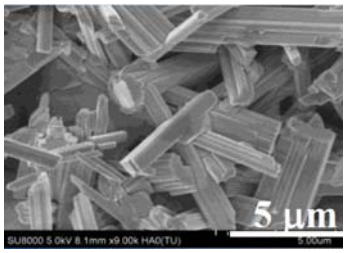

Fig. 4. SEM image of Sc-doped LTC photocatalysts.

OPERANDO SPECTROMICROSCOPY FOR 2D-ELECTRON TRANSISTORS FOR ENERGY-SAVING ICT

Hirokazu Fukidome*
*Research Institute of Electrical Communication, Tohoku University

Our FET exhibits excellent intrinsic carrier mobility >100,000 cm^2/Vs. However, degradation due to the parasitic resistance inhibits further improvement of the high-frequency characteristic toward THz operations. Further, the extrinsic carrier mobility, including the channel resistance and parasitic resistance (e.g., contact resistance), is 4,000 cm^2/Vs. Therefore, the negative contribution of the parasitic resistance must be removed. Note that the source of this phenomenon is the susceptibility of the electronic properties to the surrounding interfaces, because of the extreme thinness of graphene.

To obtain an effective science-based plan to overcome this problem, microscopic investigation of the electronic states at the interfaces related to the parasitic resistance is required; for example, at the interfaces between the graphene and metals in the source and drain electrodes. Therefore, we developed operando spectromicroscopy, i.e., x-ray spectromicroscopic observation under device operation conditions with a high spatial resolution. This was achieved using photoelectron emission microscopy (PEEM) [1] and 3D scanning photoelectron microscopy (3D nano-ESCA) [2, 3].

Since 2015, we extended the research target, GaN-HEMT, in addition to graphene transistors. GaN-HEMT utilizes a 2D electron system at an AlGaN/GaN interface. GaN-HEMT exhibits both good high-frequency characteristics (>100 GHz) and high output performances larger than those of Si by more than one order of magnitude.

However, there are some issues to be solved as a reliable millimeter-wave (30GHz-300GHz) communication devices, such as radar. Among them, drain current collapse is the main issue to acquire the high operation reliability. The drain current collapse is the discrepancy between DC and RF maximum current. The drain current collapse has been suggested to originate from electron trapping processes by surface states that exist near the gate where a local electric field is large. The problem is that microscopic mechanism of the trapping process has not been well characterized because of the lack of material characterization, although it was characterized by electrical characterization.

The purpose of this work is to microscopically and element-specifically characterize the electron trapping process by using operando 3D nano-ESCA observation. Then the solution to improve the high-reliability of GaN-HEMT will be done by feed backing operando 3D nano-ESCA observation.

Figure 1 shows the pinpoint operando observation. It is clearly shown that, near the gate where the local electric field is large, the new peak appears, in addition to the GaN main peak. Therefore, the new peak is associated with surface electron trapping which induce the current collapse. This is the first direct spectroscopic evidence of the surface electron trapping. In addition to the pinpoint spectra, we did the line profile analysis. This line

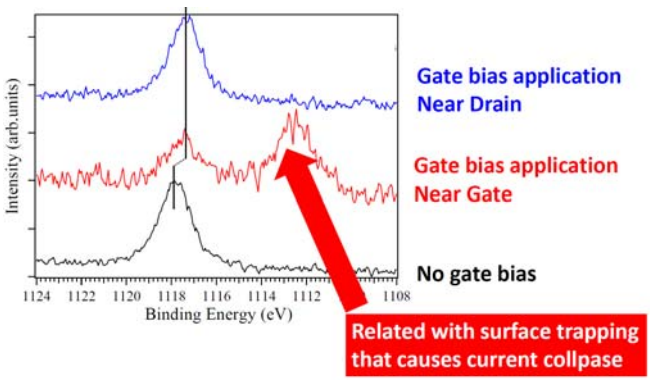

Fig. 1 The appearance of the new peak by the gate bias application near the gate.

profile analysis confirm that the new peak associated with surface electron trapping appears near the gate.

SiN surface passivation of GaN-HEMT has been shown to be effective for the suppression of the current collapse by electrical measurements. To clarify the mechanism of the suppression of the current collapse, 3D nano-ESCA observation on the effect of SiN surface passivation, as shown in Fig. 2. The SiN passivation diminishes the new peak associated with the electron trapping, while, without the SiN passivation, the new peak is present. This observation support the conclusion from Fig 1 that the new peak is associated with the current collapse. Furthermore, the role of the SiN passivation is the vanishment of the Ga species associated with the electron trapping.

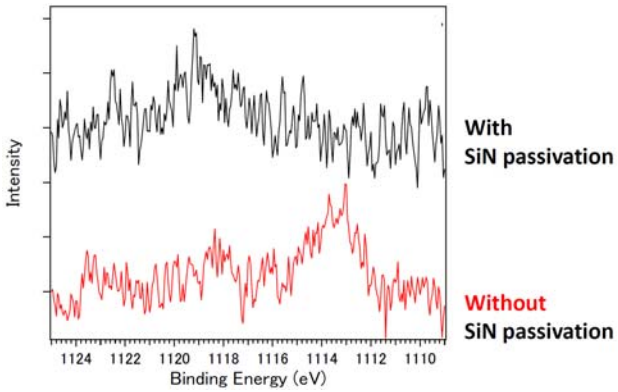

Fig. 2 The effect of the SiN passivation.

In conclusion, we successfully extended the research target of 3D nano-ESCA, GaN-HEMT, in addition to graphene transistors. The obtained results are surely useful to solve the current collapse that induces the operation instability of GaN-HEMT.

REFERENCES

[1] H. Fukidome et al., Sci. Rep. (2014).
[2] H. Fukidome et al., APEX (2014).

High-energy-resolution soft x-ray emission study of $LiCoO_2$

Takaaki Sudayama[1], Daisuke Asakura[1], Eiji Hosono[1], Jun Miyawaki[2,3], Hisao Kiuchi[4], Hideharu Niwa[2,3], and Yoshihisa Harada[2,3]

[1]*Research Institute for Energy Conservation, National Institute of Advanced Industrial Science and Technology*

[2]*Institute for Solid State Physics, The University of Tokyo*

[3]*Synchrotron Radiation Research Organization, The University of Tokyo*

[4]*Department of Applied Chemistry, The University of Tokyo*

$LiCoO_2$ is a typical cathode material for Li-ion battery. Many studies have reported that the average valence of Co reversibly changes between Co^{3+} for discharged state ($LiCoO_2$) and $Co^{3.5+}$ for charged state ($Li_{0.5}CoO_2$) in the charge-discharge process by using hard (Co *K*-edge) or soft (Co *L*-edge) x-ray absorption spectroscopy (XAS) [1-2]. Although the Co *L*-edge XAS with analyses using charge-transfer multiplet calculations provides us the information of the Co 3*d* orbital, x-ray emission spectroscopy (XES) is more appropriate to separately evaluate the electronic structures of Co^{3+} and Co^{4+} [3]. In this study, in order to investigate the electronic structure changes in charge and discharge processes for $LiCoO_2$, we performed *ex situ* Co 2*p* XAS and high-energy-resolution XES measurements.

$LiCoO_2$ powder was prepared by a sol-gel method. $LiCoO_2$ powder (75 wt %), acetylene black (20 wt %), and PTFE (5 wt %) were made into a paste and then were pressed to stainless mesh. The $LiCoO_2$ cathode was assembled with a Li-metal counter electrode, a Li-metal reference electrode and a 1M $LiClO_4$/EC-DEC electrolyte solution as a three-electrode beaker cell. Cyclic voltammetry (CV) was employed for the charge experiment. The scan speed was set to 0.5 mV/s. The cut-off voltages were 4.2 V (vs. Li/Li^+) for charge and 3.0 V for discharge, respectively. We prepared the samples of initial state before charging, charged state (4.2 V), and discharged state (3.0 V) for the first cycle. In addition, a sample of after the 6th cycle (3.0 V) was also prepared. After the samples were taken out from the cell in the grove box, they were transferred to a vacuum chamber by using a transfer vessel filled with Ar gas to avoid exposure to air. The XES and XAS experiments were carried out using ultrahigh-resolution x-ray emission spectrometer, HORNET [4] at BL07LSU of SPring-8. An excitation energy E_{in} of 779.5 eV corresponding to the main peak position of the Co L_3-edge absorption spectrum was used for XES. For the XAS measurements, total electron yield (TEY) detection mode was employed. All the XES/XAS measurements were performed at room temperature. We performed the spectral analyses for the XAS results by using the CTM4XAS software program based on the charge-transfer multiplet calculations [5].

Figure 1 shows the experimental results of Co 2*p* XAS of $LiCoO_2$ and a calculated spectrum for Co^{3+} low spin (LS) state. The spectra of the initial state, the discharged state, and the discharged state after 6th cycles have the same line shape and their shapes are consistent with the calculated spectrum of Co^{3+} LS state. The results indicate that the redox reaction of Co is reversible at least up to 6th cycle. On the other hand, in the case of the charged state, energy shift of L_3-edge peak-top toward higher energy was observed and a shoulder structure of higher energy side in L_3-edge was enhanced. The results indicate that the Co^{3+} state is partially oxidized to Co^{4+} with the charge process. The ratio of Co^{3+} to Co^{4+} would be almost even considering the cut-off voltage for the charged state is 4.2 V (in which the charge-discharge capacity is about 150 mAh/g corresponding to $0.5Li^+$ extraction).

Figure 2 shows the Co 2*p* resonant XES spectra of $LiCoO_2$ for the excitation energy of 779.5 eV. In the charge state, the XES peaks between 776.0 eV and 778.0 eV corresponding to *d-d* excitation drastically changed with increasing Co^{4+}. Also, a slight decrease of the XES spectral weight below 776.0 eV related to charge-transfer excitation for O 2*p* → Co 3*d* as compared to charged state was observed. In the near future, we will carry out the spectral analyses for the XES results by using the charge-transfer multiplet calculations.

In summary, we performed ex situ Co 2*p* XAS and high-energy-resolution XES for $LiCoO_2$. The XES results exhibited significant changes in the line shape due to a redox reaction between Co^{4+} and Co^{3+} by charge/discharge processes. It was observed that for the charged state, *d-d* excitation drastically changes with increasing Co^{4+} and the charge-transfer excitation is slightly weakened.

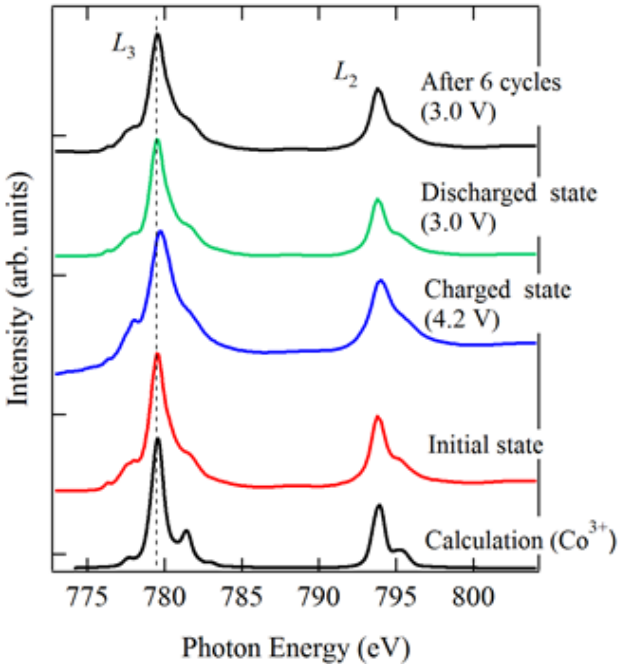

Fig. 1 Co 2*p* TEY XAS spectra for $LiCoO_2$

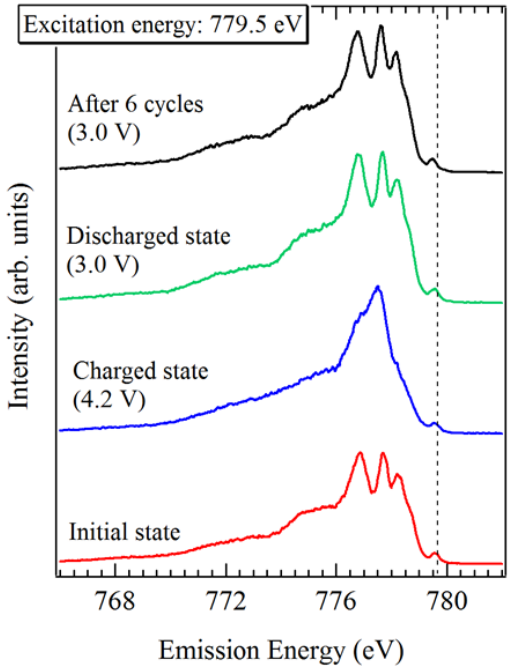

Fig. 2 Co 2*p* resonant XES spectra for $LiCoO_2$ taken with an excitation energy of 779.5 eV.

References

[1] I. Nakai *et al*., J. Power Sources **68**, 536 (1997).
[2] L. A. Montoro *et al*., Electrochem. Solid State Lett. **3**, 410 (2000).
[3] A. Kotani *et al*., Rev. Mod. Phys. **73**, 203 (2001).
[4] Y. Harada *et al*., Rev. Sci. Instrum. **83**, 013116 (2012).
[5] E. Stavitski *et al*., Micron **41**, 687 (2010).

CHARGE EXCITATIONS IN HIGH-T_C CUPRATES STUDIED BY RESONANT INELASTIC X-RAY SCATTERING AT THE OXYGEN K-EDGE

Kenji Ishii[1], Kentaro Sato[2], Masaki Fujita[2],
Jun Miyawaki[3], Hideharu Niwa[3], Yoshihsa Harada[3]
[1]*Synchrotron Radiation Research Center, National Institutes for Quantum and Radiological Science and Technology*
[2]*Intsitute for Materials Research, Tohoku University*
[3]*Synchrotron Radiation Laboratory, The Institute for Solid State Physics, The University of Tokyo*

High-T_c superconductivity in cuprates emerges when holes or electrons are doped as mobile carriers in the antiferromagnetic Mott insulator, and antiferromagnetic fluctuation is believed to be the most possible origin of the superconductivity. Therefore, comprehensive observation of charge dynamics of the doped carriers and spin dynamics of the antiferromagnetic fluctuation is a prerequisite for understanding the superconductivity. Furthermore, the doped cuprates are suitable for the study of electron dynamics in strongly correlated electron systems because only a limited number of orbitals contribute to the electronic states near the Fermi energy. Inelastic neutron scattering is traditionally used to measure spin excitations in energy-momentum space and Cu L_3-edge resonant inelastic x-ray scattering (RIXS) has recently become an alternative. Complementary use of the two inelastic scattering techniques enables one to explore the spin excitations in wide energy range [1]. On the other hand, momentum-resolved charge excitations have been studied by Cu *K*-edge RIXS so far [2] but a huge elastic tail makes it difficult to elucidate the charge excitation at low energy. Here we demonstrate that O *K*-edge RIXS is another technique to observe dispersive charge excitations in the hole-doped cuprates.

The experiment was preformed at BL07LSU of SPring-8 using the HORNET spectrometer. Total energy resolution was 190 meV. Single crystals of $La_{2-x}Sr_xCuO_4$ (x = 0, 0.075, and 0.18) were mounted so that the scattering plane is parallel to the ac-plane of the crystals and kept at the base temperature around 30 K. The scattering angle (2θ) was 90 degree and the momentum was scanned by rotating the crystals along the b-axis. In this report, we use the momentum transfer (**q**) projected on the CuO_2 plane. In the x-ray absorption spectrum (XAS) of $La_{2-x}Sr_xCuO_4$, two peaks are observed near the O *K*-edge [3]. The peak at lower energy is the O 2*p* state of doped holes (hole peak) while high-energy peak corresponds to the state hybridized with the Cu 3*d* upper Hubbard band (UHB peak). We tuned the incident photon energy to either of the peaks. The incident photon is σ-polarized.

Figure 1(a) shows O *K*-edge RIXS spectra of x = 0.18. Incident photon energy is selected at the hole peak in XAS. In contrast to the momentum-independent bimagnon excitations in the parent compound (x = 0) [4], a dispersive mode is clearly observed below 1 eV. Such a dispersive mode in sub-eV range has been also observed in electron-doped $Nd_{2-x}Ce_xCuO_4$ using RIXS at Cu *K*- and L_3-edges [1] and it is assigned to charge excitations. Furthermore, a recent theoretical calculation based on the *t-J* model predicts that dynamical charge correlation function in the sub-eV range is qualitatively similar between hole- and electron-doped cuprates [5]. Therefore we reasonably ascribe the dispersive mode to the charge origin. In Fig. 1(b), we compare the spectra of x = 0.075 taken at the incident photon energy of the hole peak (528.8 eV) and UHB peak (530.5 eV) of XAS. The dispersive mode is also observed in x = 0.075 and the spectra at the two incident photon energies are almost identical except for the intensity of elastic or quasi-elastic scattering. It confirms that the dispersive mode is a Raman feature rather than incoherent fluorescence.

It is noted that RIXS response is not necessarily the same between hole- and electron-doped cuprates because of opposite sign of the core-hole potential in the intermediate state. While

the charge excitations are observed by the Cu L_3-edge RIXS spectra for electron-doped cuprates, they have not been identified so far for hole-doped cuprates. Our result proves that O *K*-edge RIXS of hole-doped cuprates is an alternative to the Cu L_3-edge RIXS of electron-doped cuprates for the study of momentum-resolved charge excitations.

In conclusion, we succeeded to observe dispersive charge excitations in the hole-doped cuprates $La_{2-x}Sr_xCuO_4$ by the O K-edge RIXS. Combined with the Cu K-edge RIXS, we are now able to measure charge dynamics of hole-doped cuprates in wide energy-momentum space.

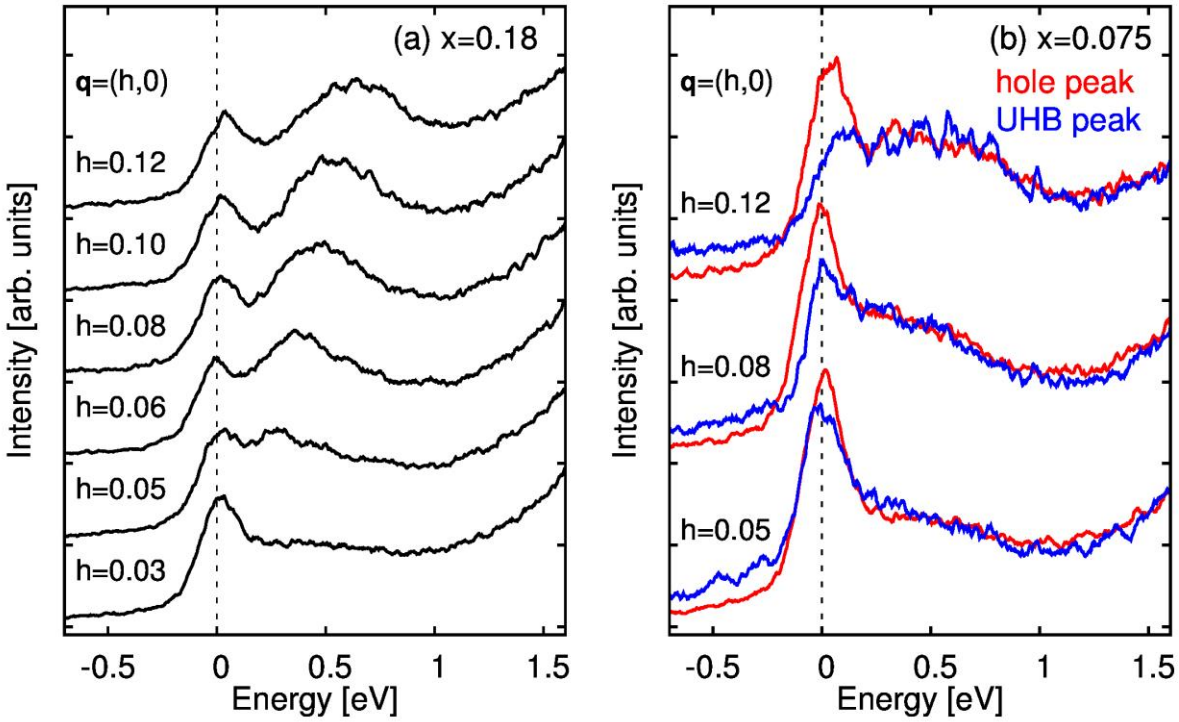

Figure 1 (a) Momentum dependence of O K-edge RIXS spectra of $La_{2-x}Sr_xCuO_4$ x = 0.18. (b) O K-edge RIXS spectra of x = 0.075. Incident photon energy is tuned to either hole peak (528.8 eV) or UHB peak (530.5 eV) in XAS.

REFERENCES

[1] K. Ishii *et al.*, Nat. Commun. **5**, 3714 (2014).
[2] K. Ishii *et al.*, J. Phys. Chem. Solids **69**, 3118 (2008).
[3] C. T. Chen *et al.*, Phys. Rev. Lett. **66**, 104 (1991).
[4] V. Bisogni *et al.*, Phys. Rev. B **85**, 214527 (2012).
[5] T. Tohyama, J. Electron Spectrosc. Relat. Phenom. **200**, (2015).
[6] R. Comin et al., Annu. Rev. Condens. Matter Phys. **7**, 369 (2016).

VALENCE FLUCTUATION IN QUANTUM CRITICAL Yb(Al,Fe)B_4 STUDIED USING SOFT X-RAY TIME RESOLVED PHOTOEMISSION SPECTROSCOPY. II

M. Okawa[1], K. Akikubo[2], S. Yamamoto[2], I. Matsuda[2], S. Shin[2], S. Suzuki[3], S. Nakatsuji[3], T. Saitoh[1]

[1]*Department of Applied Physics, Tokyo University of Science*

[2]*Synchrotron Radiation Laboratory, Institute for Solid State Physics, University of Tokyo*

[3]*Division of New Materials Science, Institute for Solid State Physics, University of Tokyo*

Introduction

In some heavy-fermion systems, the quantum critical point (QCP), which is the second-order phase transition point or first-order transition end point at absolute zero, can be induced by non-thermal parameters, i.e., magnetic field, pressure, and chemical doping. QCP is strongly attractive in the condensed matter studies because a quantum fluctuations associated with QCP can cause exotic phenomena such as non-Fermi liquid metallic state and unconventional superconductivity [1]. β-$YbAlB_4$ is the first-discovered heavy-fermion superconductor (T_c = 80 mK) in Yb-based systems [2], and is just at the QCP (or the quantum critical phase) under ambient pressure and zero field [3]. In addition, the Fermi-liquid metal α-$YbAlB_4$, which is another polymorph of β-$YbAlB_4$, shows the same quantum criticality with the β-phase by slight doping (~1.4%) of Fe to the Al site [4]. According to a hard x-ray photoemission study [4], this QCP coexists with the unprecedented strong valence fluctuation (the Yb valence of <2.8+), which cannot be explained by the conventional Doniach phase diagram, suggesting the role of the valence instability for the quantum critical phenomena. Furthermore, a recent Mössbauer spectroscopy study [6] reported that the valence fluctuation in the $YbAlB_4$ system shows the very slow time scale of a few nanoseconds, which may be a manifestation of the valence quantum criticality. In order to investigate the relaxation dynamics of the valence fluctuating phenomena in α-$YbAl_{1-x}Fe_xB_4$, we performed soft x-ray time-resolved photoemission spectroscopy (SX-TRPES) of the whole valence band in which both Yb^{2+} and Yb^{3+} components of the Yb 4*f* state are included.

Experiment

Single crystals of α-$YbAl_{1-x}Fe_xB_4$ with x = 0 (Fermi liquid-like), 0.013 (quantum critical), 0.098 (antiferromagnetic) were grown by the Al-flux method SX-TRPES experiments were carried out at BL07LSU of SPring-8 using a VG Scienta ARTOF 10k analyser. The repetition rate of pump laser pulses (1.5 eV) was 1 kHz. The photon energy of probe synchrotron pulses was set to 253 eV. To obtain clean crystal surfaces, we fractured samples *in situ*. All data were recorded at the sample temperature of ~20 K. The Fermi level (E_F) was aligned using the valence band spectrum in α-$YbAlB_4$ recorded using hard x-ray photoemission spectroscopy at BL47XU.

Results

Figure 1(a) shows the valence-band spectrum without pump pulses in the x = 0 sample. Using the photon energy of 253 eV, the bulk 4*f* structure of both Yb^{2+} (near E_F) and Yb^{3+} (5-12 eV) were appeared in the valence-band spectrum. The surface 4*f* state, which are at slightly higher-energy side of the bulk Yb^{2+} structure as very broad peaks, was not observed. For the x = 0.013 and 0.098 samples, we obtained the results similar to that of the x = 0 sample. Thus, we can investigate the relaxation dynamics of the bulk 4*f* state in α-$YbAl_{1-x}Fe_xB_4$ using SX-TRPES.

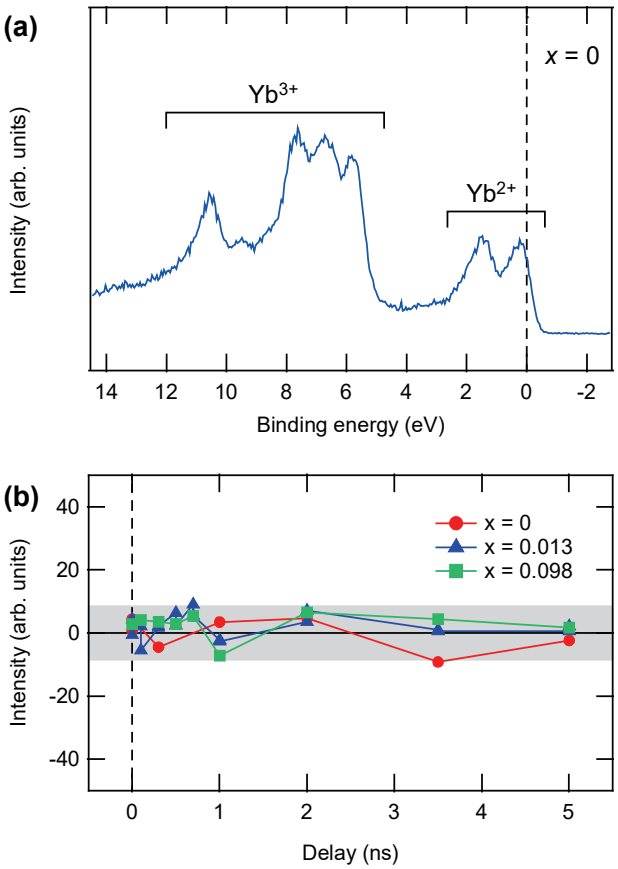

Fig. 1: (a) The valence-band spectrum of α-$YbAl_{1-x}Fe_xB_4$ (x = 0). (b) Delay-time dependence of the Yb^{3+} intensity in the x = 0, 0.013, and 0.098 samples. The shaded area indicates uncertainty in intensity determinations.

Figure 1(b) shows the delay-time (t) dependence of the Yb^{3+} intensity in the x = 0, 0.013, and 0.098 samples. The intensity was determined as the integrated intensity at the energy region of the Yb^{3+} 4*f* structure, which is shown in Fig. 1(a), of the difference spectra between pumped and $t < 0$ measurements. The uncertainty in intensity determinations, which was estimated from the difference spectra of the measurements in the same condition at $t < 0$, is appeared as the shaded area. For the all samples, as shown in Fig. 1(b), the difference intensity is in the range of the uncertainty in the measured t range. Therefore, in the relaxation dynamics of the Yb valence in quantum critical α-$YbAl_{1-x}Fe_xB_4$, the very slow process with the nanosecond time scale does not exist. To clarify the electron dynamics and its relation with the quantum critical phenomena in α-$YbAl_{1-x}Fe_xB_4$, our results suggest that more fast time scale investigations of the electronic structure are desired, e.g., using extreme ultraviolet laser based TRPES.

REFERENCES

[1] P. Gegenwart, Q. Si, and F. Steglich, Nature Phys. **4**, 186 (2008).
[2] S. Nakatsuji *et al.*, Nature Phys. **4**, 603 (2008).
[3] Y. Matsumoto *et al.*, Science **331**, 316 (2011).
[4] K. Kuga, Ph.D. thesis, University of Tokyo (2011).
[5] M. Okawa *et al.*, Phys. Rev. Lett. **104**, 247201 (2010).
[6] T. Kobayashi, JPS 2013 Autumn Meeting, 27pEC-3 (2013).

DEVELOPMENT OF PICOSECOND TIME-RESOLVED PHOTOELECTRON HOLOGRAPHY

Kouichi Hayashi*
Department of Physical Science and Engneering, Nagoya Institute of Technology

Iwao Matsuda, Hiroki Wadati, Susumu Yamamoto
Synchrotron Radiation Laboratory, The Institute for Solid State Physics, The University of Tokyo

Takayuki Muro, Tomohiro Matsushita
Japan Synchrotron Radiation Research Institute/ SPring-8

Yoshihito Tanaka
Graduate School of Material Science, University of Hyogo

1. Introduction

As represented by dopants in semiconductors, in most of materials have active sites, providing novel functions. To reveal atomic structures of the active sites, we have conducted researches of atomic resolution holography for various functional materials, because the atomic resolution holography provides 3D atomic images around specific elements within a few nm in a radius.[1] However, all of its achievements are about static structures. Therefore, we have planned time-resolved atomic resolution holography. Since we thought that the surface structural change induced by laser can be observed by photoelectron holography, among various atomic resolution holography methods, photoelectron holography is surface sensitive.

In the present experiment, we chose VO_2 thin films as a measure sample. And, we tried to observe time-resolved photoelectron holograms.[2,3]

2. Experimental

The experiment was carried out at BL07LSU in SPring-8. The operation mode was D-mode (1/7 filling+5 bunches). We used the third bunch at each period to synchronize the femtsecond laser pulse (38.6 mW). For the adjustment of the x-ray bunch and the laser pulse, we used the photoelectron signals Si (111).

Subsequently, we measured valence band (VB) photoelectron spectra from the VO_2 thin films with the incident energy of 253 eV. The delayed time was 0, 0.05, 0.1, 0.2, and 1.0 nm. The sample temperature was maintained at 230 K. Then, we measured V3p peak with the incident energy of 700 eV at room temperature and 240K. The acquisition time at room temperature and 240 K were 1 h and 10 h, respectively. The measured sample of the VO_2 thin film was fabricated at Muraoka laboratory in Okayama laboratory. The transition temperature in the films was 295 K on heating cycle and 285 K on cooling cycle, while the MIT occurs at 340 K in bulk samples.[3]

3. Results and discussion

Figure 1(a) shows the VB photoelectron spectrum at 0.1 ns delayed time. For comparison, the spectrum without laser irradiation was plotted together. Whole of the laser-ON spectrum was shifted by 0.5 eV. Similar phenomenon was observed for the 1.0 s delayed spectrum as shown in Fig.1 (b). The spectra of the VB were recovered at the next bunches (+684.3 ns).

Initially, the reason of these shifts is considered to be charge-up of the sample

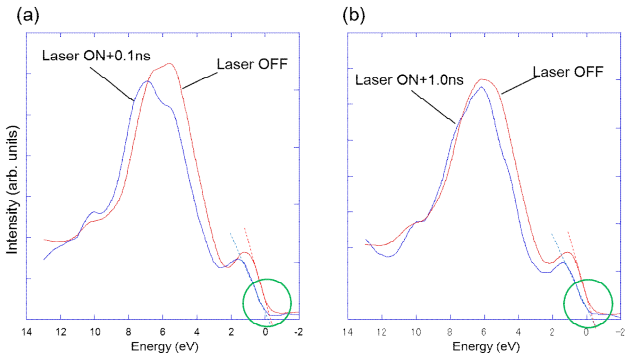

Fig.1 Valence band spectra of VO_2 after laser irradiations.

due to strong laser irradiation. However, the values of the edges of the spectra for laser-ON and OFF are mostly same, as indicated by circles in Fig.1. This shows that the charge-up is not intrinsic reason. Thus, further discussion is necessary to understand the spectrum modification owing to the laser irradiation.

Figure 2 shows the V 3p and O 2s photoelectron holograms at room temperature and 230 K, at which the VO_2 thin films exhibit metallic and insulator phases, respectively. Since visibilities of these patterns at room temperature and 240 K are largely different due to the difference of acquisition times, it is difficult to discuss quantitatively structures at the metallic and insulator phases. If we can enhance the statistics of the hologram data by the symmetric manipulation using the crystallographic symmetry of the sample surface, more quantitative discussion will be possible.

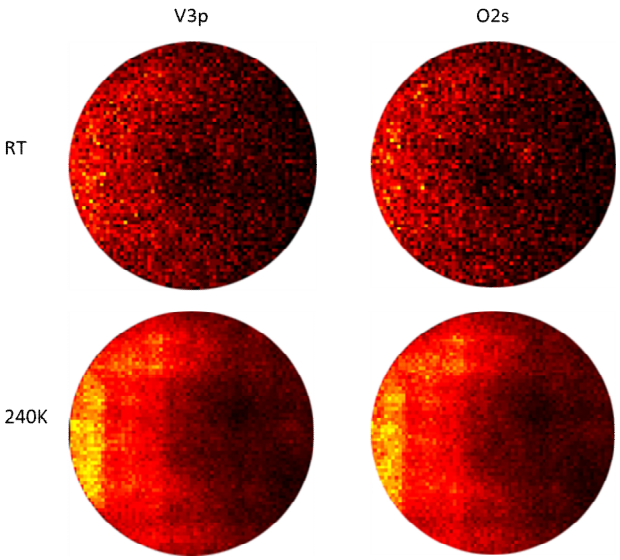

Fig.2 Photoelectron holograms of V 3p and O 2s at room temperature and 240 K.

4. Conclusion

We tried to carry out the time-resolved photoelectron holography experiments using the VO_2 epitaxial thin film samples. The changes of the photoelectron spectra were clearly observed owing to the laser irradiation. However, we knew that the photoelectron yields were not enough to observe the hologram patterns in the time-resolved experiments, because number of the events is much less than that in normal photoelectron holography experiments. This problem will be resolved with a 200 kHz laser.

REFERENCES

[1] K. Hayashi, N. Happo, S. Hosokawa, W. Hu, and T. Matsushita, J. Phys.: Condens. Matter 24, 093201 (2012).
[2] M. Hada, K. Okimura, and J. Matsuo, Phys. Rev. B 82, 153401 (2010).
[3] K. Okazaki, H. Wadati, Fujimori, M. Onoda, Y. Muraoka, and Z. Hiroi, Phys. Rev. B 69, 1651041 (2004).

EFFECT OF OXYGEN VACANCIES ON THE PHOTOEXCITED CARRIER LIFETIME ON TITANIUM DIOXIDE SURFACES

Kenichi Ozawa[1], Susumu Yamamoto[2], Roya Liu[2], Koki Inoue[3], Taku Higuchi[3], Hiroshi Sakama[3], Kazuhiko Mase[4,5], Iwao Matsuda[2]

[1]*Department of Chemistry, Tokyo Institute of Technology*

[2]*Synchrotron Radiation Laboratory, The Institute for Solid State Physics, The University of Tokyo*

[3]*Department of Physics, Sophia University*

[4]*Institute of Materials Structure Science, High Energy Accelerator Research Organization*

[5]*SOKENDAI (The Graduate School of Advanced Studies)*

INTRODUCTION

A novel property of titanium dioxide (TiO_2) as a photocatalyst has attracted considerable interests from both scientific and industrial communities since the discovery of the Honda-Fujishima effect. The photocatalytic activity is initiated by absorption of the ultraviolet light and creation of excited carriers (electrons and holes in the conduction and valence bands, respectively), which diffuse to the surface and interact with adsorbed chemical species. Therefore, extensive efforts have been devoted to elucidate dynamics of excited carriers by various time-resolved techniques such as absorption spectroscopy, reflectance spectroscopy, photoluminescence measurements, conductivity measurements, photoelectron spectroscopy, etc.

It has been considered that there is a correlation between the photocatalytic activity and the carrier lifetime, i.e., the longer the lifetime is, the higher the activity is. In our recent study using time-resolved photoelectron spectroscopy (TRPES) [1], a relevance between the surface potential, which acts as a barrier for the carriers to be transported from the bulk to the surface, and the carrier lifetime has been examined for anatase and rutile TiO_2 single crystal surfaces. It is found that, although the carrier lifetime is greatly influenced by the barrier height, the carriers are expected to survive longer on the anatase surface than on the rutile surface if the potential heights are nearly equivalent on these surfaces. The longer lifetime on the anatase surface correlates well with the higher photocatalytic activity of anatase TiO_2 in comparison with rutile TiO_2.

The next question is what are determining factors of the carrier lifetime beyond the surface potential. To answer this question, we compared the carrier lifetimes on the rutile TiO_2(110) surfaces with different O vacancies. Influence of the carrier trap states and the carrier trap cross section on the carrier lifetime is verified by TRPES.

EXPERIMENTAL

The TRPES measurements by a pump-probe method were carried out at SPring-8 BL07LSU (Proposal No. 2015A7487). The photon energies of the pump laser and the probe synchrotron radiation were 3.06 eV and 600 eV, respectively. The rutile TiO_2(110) surface was cleaned by cycles of Ar^+ sputtering and annealing in O_2 atmosphere. The clean (110) surfaces exhibited a 1×1 low energy electron diffraction patterns, respectively. The O vacancies on the (110) surface were created by mild Ar^+ sputtering with an ion beam energy of 1.25 kV for 10 min.

RESULTS AND DISCUSSION

Ar^+ sputtering of TiO_2 preferentially removes O atoms from the surface and forms Ti^{3+} species, which give a state at 457 eV in the Ti $2p_{3/2}$ core-level region (Fig. 1a). The amount of the Ti^{3+} species is estimated from the Ti^{3+} peak intensity to be 2.6×10^{21} cm^{-3}, which is about 4 times larger than that on the surface before sputtering. The Ti^{3+} species also give a state in the band-gap region (Fig. 1b), and this state should act as an carrier tarp state when the photoexcited carriers are generated. Thus, it is expected that a larger amount of Ti^{3+} leads to the shorter carrier lifetime. However, the estimated lifetime on the sputtered surface is longer (300 ns) than on the pre-sputtered surface (50 ns), as shown in Fig. 2. This discrepancy is understood if the potential barrier height at the surface is taken into account.

On both sputtered and pre-sputtered surfaces, the TiO_2 bands are bent downwardly with magnitudes of band bending of respectively 0.55 eV and 0.4 eV, which are equivalent to the barrier heights, The larger barrier height on the sputtered surface makes the photogenerated holes reach to the surface much less frequently. Thus, the electron-hole recombination is suppressed at the surface, and the longer carrier lifetime is realized. If the flat band condition is realize, the carrier lifetimes should be 0.2 ps and 2 ps on the sputtered and pre-sputtered surfaces, respectively. The shorter lifetime on the sputtered surface is a consequence of a larger density of the Ti^{3+}-derived carrier trap state.

The flat-band carrier lifetime τ_0 is given by $\tau_0 = 1/(\sigma_p v_p N_p)$, where σ_p, v_p, N_p are a capture cross section of the carriers, a carrier thermal velocity and a density of the carrier trap states (a subscript p means that the carriers are the holes). Taking $v_p = 6.7\times10^6$ cm/s, which is a typical value for the holes in TiO_2, we obtain the hole capture cross section $\sigma_p = 3\times10^{-16}$ cm^2 for the sputtered surface ($N_p = 2.6\times10^{21}$ cm^{-3} and $\tau_0 = 0.2$ ps). On the other hand, when we use the values for the pre-sputtered surface ($N_p = 2.6\times10^{21}$ cm^{-3} and $\tau_0 = 2$ ps), σ_p is evaluated to be 1×10^{-16} cm^2. The obtained σ_p values coincide reasonably with each other, indicating that the electron-hole recombination occurs via hole trapping by the Ti^{3+} state in the band gap with the hole cross section in the order of 10^{-16} cm^2. The electron capture cross section has been reported to be 10^{-17}—10^{-16} cm^2 [2]. Thus, there is no significant difference of the cross sections between the electrons and the holes on the TiO_2 surfaces.

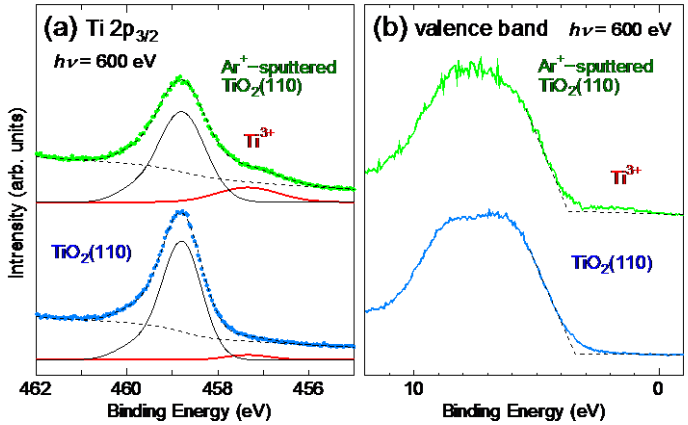

Fig. 1 (a) Ti $2p_{3/2}$ and (b) valence band spectra of pre- and post-sputtered TiO_2(110) surfaces.

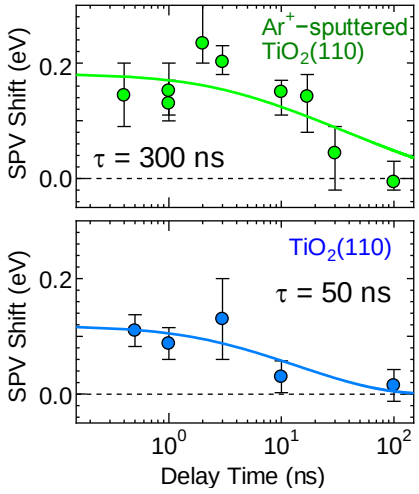

Fig. 2 Time-dependent surface photovoltage (SPV) shifts. The SPV shifts were determined by tracing the Ti $2p_{3/2}$ peak shifts.

REFERENCES

[1] K. Ozawa *et al.*, J. PHYS. CHEM.. LETT. **5**, 1953 (2014).
[2] R. H. Wilson, J. ELECTROCHEM. SOC. **127**, 228 (1980).

ANALYSIS OF STRUCTURES AND ELECTRONIC STATES OF [ACTIVE-SITE] IN FUNCTIONAL MATERIALS BY MICROSCOPIC HIGH-RESOLUTION TWO-DIMENSIONAL PHOTOELECTRON SPECTROSCOPY

Hiroshi Daimon*, Yusuke Hashimoto, Mihee Lee, Shun Fukami, Daichi Tsujikawa, Taisuke Yoshida, Hiroyuki Matsuda, Munetaka Taguchi

Graduate School of Materials Science Laboratory, Nara Institute of Science and Technology

The main purpose of our study at BL07LSU is to develop and establish the experimental methods for structural and electronic states studies by using two-dimensional microscopic photoelectron diffraction spectroscopy, so-called DELMA [1,3]. We have so far developed a two-dimensional display-type ellipsoidal mesh analyzer (DELMA), which is composed of a wide acceptance angle electrostatic lens (WAAEL) unit, a transfer lens system and a high energy electron analyzer (VG SCIENTA R4000) at SPring-8 BL07LSU [1]. DELMA is a photoelectron spectroscopy device that has the photoelectron emission microscope function, spatial resolution about 100 μm now, which allows us to measure two dimensional photoelectron intensity angular distribution (2D-PIAD) of the individual small regions in the sample microscopically. The acceptance angle of the photoelectron angular distribution pattern is ±45°, and the total energy resolution ΔE/E of DELMA combined with a concentric hemispherical analyzer is 0.2% at kinetic energy around 700 eV.

In 2015A beam-time, we have measured the photoelectron diffraction of Ir doped $LaAlO_3/SrTiO_3$ (LAO/STO) interface. The interface of transition metal oxide shows the various interesting physical properties of the electric conductivity, superconductivity and the ferromagnetism. The observation of a metallic conductivity between two insulating perovskite type oxides, especially LAO/STO, has enhanced the potential of oxides for electronics [4]. LAO and STO is wide-gap insulator, however these interface shows metallic conductivity. It is expected as environmental low load type high electron mobility transistor (HEMT) instead of the conventional As compound. On the other hand, the *5d* transition metal oxides attract much interest for novel properties arising from the interplay between strong spin-orbit interaction and electronic correlation. These materials, which include the Ir oxides, are expected to act as topological insulators [5], [6]. The present study aims to investigate effect of doped Ir on metallic conductivity at STO/LAO interface and find out the mechanism of the phenomenon by analysis of electric state and structure.

LAO/STO and Ir doped LAO/STO interface were grown by Pulsed Laser Deposition (PLD) using a single crystal $LaAlO_3$, IrO_2 and Ir doped $SrTiO_3$ targets on STO (001) single crystal substrates. 2D-PES measurements were performed at the free port of BL07LSU in SPring-8. The DELMA combined with an energy analyser (VG SCIENTA R4000) was used to obtain two dimensional photoelectron intensity distribution (2D-PIAD) patterns. Figure 1 show 2D-PIAD patterns of Sr *3d*, Ti *2p*, O *1s*, La *4p*, Al *2p*, and Ir *4f* in 1% Ir doped STO/LAO, respectively. Each pattern shows 4-fold symmetry, consistent with the tetragonal crystal structure of STO/LAO. From Fig. 1, we clearly see that La *4d* and Sr *3d* PIAD patterns are quite similar, but O *1s* PIAD patterns is different from them, suggesting the difference of the local atomic structure between O atom and other atoms, while we could not observe the Ti *2p* PIAD. Figure 1 also shows that the doped Ir *4f* PIAD pattern is similar to that of Sr *3d* pattern, which suggests that the Ir atom will be substituted in Sr site. The observation of doped Ir *4f* PIAD strongly suggest that the local structure information on the dopant site will be successfully obtained by DELMA.

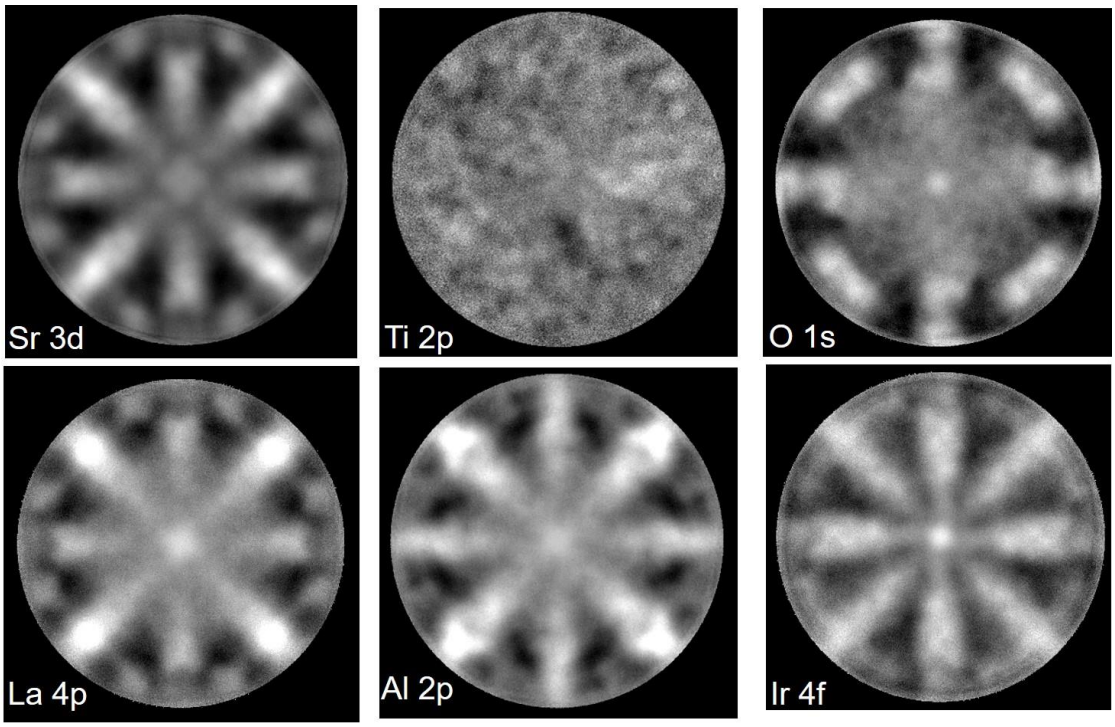

Figure 1 The measured photoelectron diffraction patterns for Sr *3d,* Ti *2p*, O *1s*, La *4p* and Al *2p* and Ir *4f.*

ACKNOWLEDGMENT

This work was supported by KAKENHI (Grants No. 26105001).

REFERENCES

[1] L. Tóth, *et al.*, J. Vac. Soc. Jpn. **51**, 135 (2008).
[2] K. Goto, *et al.*, e-J. Surf. Sci. Nanotech. **9**, 311-314 (2011).
[3] L. Toth, *et al.*, Nucl. Inst. Meth. Phys. Research Sec. A **661**, 98-105 (2012).
[4] A. Ohtomo *et al.*, Nature **427**, 423 (2004).
[5] B. J. Kim *et al.*, Phys. Rev. Lett. **101**, 076402 (2008).
[6] D. Xiao *et al.*, Nat. Commun. **2**, 596 (2011).
[4] M. Taguchi *et al.*, Phys. Rev. Letts. **100**, 206401 (2008).

RIXS of α-Fe_2O_3 in magnetic field

J. Miyawaki[1,2], S. Suga[3], H. Fujiwara[4], H. Niwa[1,2], H. Kiuchi[5] and Y. Harada[1,2]

[1]*The Institute for Solid State Physics (ISSP), The University of Tokyo, Japan,*
[2]*Synchrotron Radiation Research Organization, The University of Tokyo, Japan,*
[3]*Institute of Scientific & Industrial Research, Osaka University, Osaka, Japan,*
[4]*Graduate School of Engineering Science, Osaka University, Osaka, Japan,*
[5]*Department of Applied Chemistry, The University of Tokyo*

Dzyaloshinskii-Moriya (DM) interaction, which is originated from spatial inversion symmetry breaking, plays an important role in the magnetoelectric-effect of mutiferroic materials and both experimental and theoretical studies have been intensively carried out. Typical weak ferromagnetic material, α-Fe_2O_3 has the corundum structure and is an antiferromagnet: Below the Morin temperature (T_M), spin moments align along [111] direction of the rhombohedral lattice, while above T_M the (spin) moments show spin reorientation to the basal plane and are slightly canted due to DM interaction, resulting in weak ferromagnetism. In this study, magnetic circular dichroism (MCD) in Fe *L*-edge soft x-ray resonant inelastic x-ray scattering (SX-RIXS) of α-Fe_2O_3(111) single crystal was measured at room temperature (RT) to identify the electronic structure and mechanism inducing weak ferromagnetism.

SX-RIXS spectra were obtained at ultrahigh-resolution soft x-ray emission spectroscopy station at BL07LSU in SPring-8 [1,2] where a measurement system for MCD in SX-RIXS has been developed. Magnetic fields of ~0.25 T can be applied to a sample placed at the center of the magnetic poles. The magnet can be rotated around the axis perpendicular to the x-ray scattering plane, and SX-RIXS can be obtained by applying the magnetic field parallel and 45 degrees to the incident x-ray. A dedicated sample stage was designed to be as small as possible to allow RIXS measurements at arbitrary incident angles by rotating the stage between the magnetic poles. MCD in RIXS was measured at RT with grazing incidence (10 degree from the sample surface) and the magnetic field was set parallel to the incident x-ray.

Figure 1 shows (a) Fe $L_{3,2}$-edge x-ray absorption spectroscopy (XAS) and (b) SX-RIXS in magnetic field at $h\nu$ = 713.25 eV with left and right circular polarizations (LCP and RCP) of α-Fe_2O_3. The XAS spectrum shows good agreement with previous experimental results and calculations [3,4]. Because total magnetic moment of α-Fe_2O_3 is too small for MCD in XAS to detect, any discernible MCD in XAS was not observed. Ultrahigh energy resolution enabled us to distinguish 1.3 and 1.8 eV inelastic components, corresponding to *dd* transition of $^6A_{1g} \rightarrow {}^4T_{1g}$ and $^6A_{1g} \rightarrow {}^4T_{2g}$ [5,6]. Circular polarization dependence of RIXS was observed only at 1.8 eV energy loss and was confirmed as MCD by the reverse of the sample magnetization. The MCD in RIXS was not observed main peaks in XAS of $h\nu$ = 708.2 eV and 709.8 eV. The shoulder peak at $h\nu$ = 713.25 eV in XAS is attributed to charge transfer transition. Although MCD in XAS was not observed, MCD in RIXS was only observed at $h\nu$ = 713.25 eV. These results suggests that coordinated oxygen atoms plays a significant role in the RIXS intermediate process and induces MCD in RIXS.

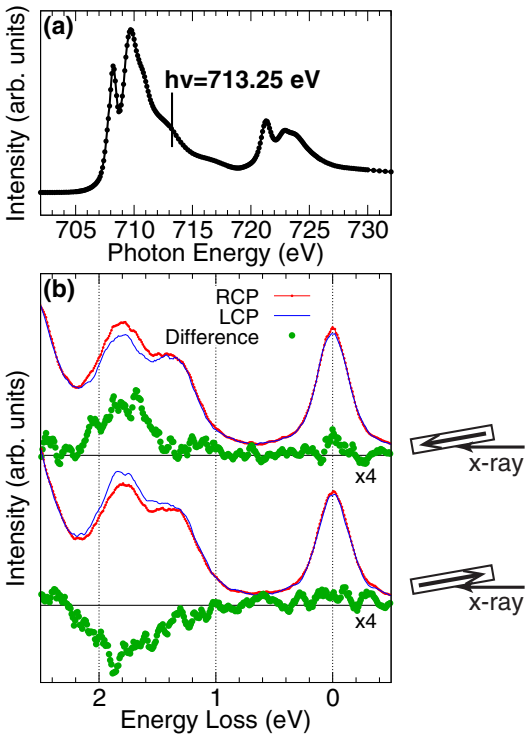

Fig. 1 Fe *L*-edge XAS and MCD in RIXS of α-Fe_2O_3. (a) Fe $L_{3,2}$-edge XAS measured in TEY. (b) Fe 2*p* RIXS measured at $h\nu$ = 713.25 eV using left and right circularly polarized x-rays. Sketch depicts the experimental configuration; arrows in the rectangles represent the directions of the magnetization.

REFERENCES

[1] Y. Harada *et al.*, *Rev. Sci. Instrum.* **83**, 013116 (2012).
[2] S. Yamamoto *et al.*, *J. Synchrotron Rad.* **21**, 352 (2014).
[3] P. Kuiper *et al.*, *Phys. Rev. Lett.* **70**, 1549 (1993)
[4] H. Kurata *et al.*, *J. Electron Microsc.* **47** 293 (1998).
[5] L. A. Marusak *et al.*, *J. Phys. Chem. Solids* **41**, 981 (1980)
[6] A. I. Galuza *et al.*, *Low Temp. Phys.* **24**, 716 (1998).

CO_2 ADSORPTION ON THE OXYGEN-MODIFIED EPITAXIAL GRAPHENE SURFACE AT NEAR AMBIENT CONDITIONS

Susumu Yamamoto[1], Kaori Takeuchi[1], Ro-Ya Liu[1], Yuichiro Shiozawa[1], Takanori Koitaya[1], Takashi Someya[1], Keiichiro Tashima[2], Hirokazu Fukidome[2], Kozo Mukai[1], Shinya Yoshimoto[1], Maki Suemitsu[2], Jun Yoshinobu[1], Iwao Matsuda[1]

[1] *The Institute for Solid State Physics, The University of Tokyo*

[2] *Research Institute of Electrical Communication, Tohoku University*

Introduction

Graphene, a two dimensional honeycomb lattice of carbon atoms, has great promise in a wide range of applications including electronic devices, sensors, energy storage, and catalysis, because of its exceptional electrical, optical, mechanical, and chemical properties. However, pristine graphene shows limitations in its direct use in these applications. For example, graphene is a zero band-gap material although semiconducting character with band-gap is required for device applications. In addition, pristine graphene is a chemically inert material, which shows weak interactions with adsorbed molecules. In order to overcome these limitations, significant efforts have been dedicated to control the electronic and chemical properties of graphene by a chemical modification or functionalization of the graphene surface.

Adsorption of molecules on the functionalized graphene is fundamentally important because adsorbed molecules on the graphene devices working at ambient conditions can have a large influence on their performances. In catalyst applications, graphene serves as catalysis or catalysis support. It is important to reveal the adsorption and chemical reactions of molecules on the graphene surface at the working conditions of catalysts. Despite of importance, however, experimental approach to clarify the interaction of adsorbed molecules with the functionalized graphene is quite limited. Especially, it has been challenging to experimentally study the graphene surface at ambient conditions where the devices and the catalysts are operated. Recent development of ambient pressure X-ray photoelectron spectroscopy (AP-XPS) allows one to investigate the electronic and chemical states of adsorbate and substrate under gas atmosphere of near ambient pressure.

In this study, the adsorption of CO_2 with the oxygen-modified graphene surface was studied at near ambient conditions using AP-XPS. We found that the oxygen-modification of graphene enhances the adsorption energy of CO_2.

Experimental method

The experiments were performed at the soft X-ray undulator beamline BL07LSU at SPring-8. The graphene sample used in this study was monolayer epitaxial graphene grown on a 6H-SiC(0001) substrate. The graphene surface was cleaned by annealing at 773 K for 30 min in UHV to remove surface contaminants, and the surface cleanness was confirmed by C 1s and O1s XPS spectra. The oxygen-modified graphene was prepared *in-situ* by photo-induced dissociation of CO_2 on graphene with strong synchrotron X-ray. XPS measurements at near ambient pressures were carried out using an AP-XPS apparatus that combines a differentially pumped electron analyzer (SPECS, PHOIBOS 150 NAP) with an ambient-pressure gas cell. The details of the AP-XPS apparatus can be found in our previous publication [1].

Results and discussion

First the adsorption of CO_2 on the pristine epitaxial graphene surface at near ambient conditions was studied using AP-XPS. Figures 1(a) and (b) show C 1s and O 1s XPS spectra of graphene measured in $p(CO_2)$= 1.5 mbar at 177 K. The main C 1s peak at 284.8 eV binding energy (BE) is assigned to graphene; the shoulder feature at 283.8 eV is ascribed to the SiC substrate. Peaks at 293.5 eV in C 1s and 536.9 eV in O 1s XPS spectra originate from gas-phase CO_2. However, no adsorbate was observed on the graphene surface under the present condition.

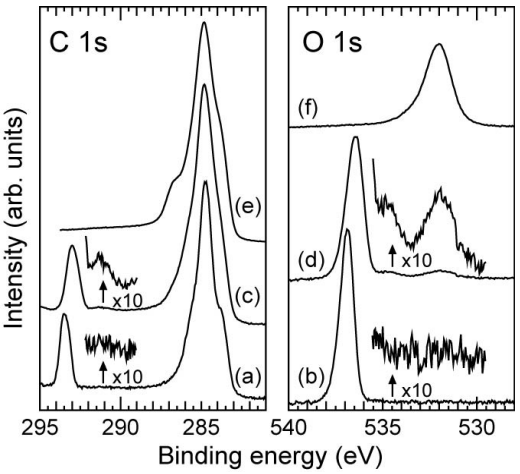

Figure 1. (a, b) C 1s and O 1s XPS spectra of graphene measured in 1.5 mbar CO_2 at 177 K. (c, d) C 1s and O 1s XPS spectra of the oxygen-modified graphene measured in 1.6 mbar CO_2 at 175 K. (e, f) C 1s and O 1s XPS spectra of the oxygen-modified graphene measured in ultrahigh vacuum at 199 K after evacuating 1.6 mbar CO_2. The incident photon energy was 740 eV.

Next the adsorption of CO_2 on the oxygen-modified epitaxial graphene surface was studied at near ambient conditions. Figures 1(c) and (d) show C 1s and O 1s XPS spectra of the oxygen-modified graphene surface measured in $p(CO_2)$= 1.6 mbar at 175 K. In contrast to the pristine graphene surface, new small peaks are observed at 291.2 eV in C 1s and at 534.7 eV in O 1s XPS spectra. The BEs are in good agreement with those of the physisorbed CO_2 on the graphene/SiC(0001) in UHV and at 30 K: 290.6-291.3 eV in C 1s and at 534.6-535.0 eV in O 1s XPS [2] . It is thus suggested that the adsorption of CO_2 on the epitaxial graphene at near ambient conditions is classified into physisorption as in UHV at 30 K. In addition to adsorbed CO_2 peaks, extra peaks are observed at 532.0 eV in O 1s and 286.7 eV in C 1s XPS spectra. The peak positions are in good agreement with the previously reported epoxide species on graphene [3]. Figures 1(e) and (f) show C 1s and O 1s XPS spectra measured in UHV after evacuating CO_2 gas atmosphere. After gas evacuation, adsorbed CO_2 as well as gas-phase CO_2 are not observed. Therefore, CO_2 molecules on the oxygen-modified graphene surface are only present at near ambient conditions.

In conclusion, the adsorption of CO_2 with the oxygen-modified graphene surface was investigated at near ambient conditions using AP-XPS. The oxygen modification of graphene was achieved *in-situ* by photo-induced dissociation of CO_2 with strong synchrotron X-ray. The oxygen-species on the graphene surface is ascribed to epoxide. Under near ambient conditions of 1.6 mbar CO_2 gas pressure and 175 K sample temperature, no CO_2 adsorption is observed on the pristine graphene, but CO_2 adsorption is observed on the oxygen-modified graphene surface. Therefore, the oxygen-modification of graphene enhances the adsorption energy of CO_2. The results of the present study may present the guideline of novel graphene-based catalysts design; the adsorption of reactant molecules should be increased by the functionalization of the graphene surface.

REFERENCES

[1] T. Koitaya *et al.*, Topics in Catalysis **59**, 526 (2016).
[2] K. Takeuchi *et al.*, submitted (2016).
[3] Md. Z. Hossain *et al.*, Nature Chemistry **4**, 305 (2012).

ACTIVATION OF CARBON DIOXIDE ON Zn-DEPOSITED Cu SURFACES STUDIED BY AMBIENT-PRESSURE X-RAY PHOTOELECTRON SPECTROSCOPY

Yuichiro Shiozawa, Takanori Koitaya, Susumu Yamamoto, Kaori Takeuchi, Ro-Ya Liu, Kozo Mukai, Shinya Yoshimoto, Yuki Yoshikura, Iwao Matsuda, and Jun Yoshinobu*

* *The Institute for Solid State Physics, The University of Tokyo*

Activation of CO_2 is an important reaction step in the use of CO_2 as a chemical feedstock [1, 2]. So far, methanol synthesis on a Cu/ZnO catalyst has been one of the most promising reactions for the CO_2 utilization [3]. It has been proposed that an active site on the Cu/ZnO catalyst is a Zn-Cu surface alloy formed by diffusion of Zn atoms to metallic copper [4]. A recent study has suggested that a step site on the Cu surface decorated with Zn is highly reactive for the methanol synthesis [5]. However, the reaction mechanism and kinetics of CO_2 on the Zn-Cu alloy surface are not fully understood yet. In this study, we investigated the reaction process of CO_2 on the Zn-deposited Cu(111) and Cu(997) surfaces at 373 K using ambient pressure X-ray photoelectron spectroscopy (AP-XPS).

AP-XPS is a powerful tool for investigating electronic structures and chemical states of adsorbates and substrates under reactant-gas atmosphere. We have constructed the ambient pressure X-ray photoelectron spectroscopy system at the "free-port" of the soft X-ray undulator beamline BL07LSU of SPring-8. Details of the system are described elsewhere [6]. Briefly, the AP-XPS system consists of four interconnected UHV chambers; an analysis chamber, a preparation chamber, a load-lock chamber, and a fast-entry chamber. The analysis chamber is used for XPS measurements both in UHV and at ambient conditions using a gas-cell. The preparation chamber is equipped with an ion source and low energy electron diffraction (LEED) optics. The load-lock chamber and the fast-entry chamber allow the introduction of samples from the air into the UHV system.

Figure 1 shows a series of C 1s AP-XPS spectra on (a) Zn(0.31 ML)/Cu(111) and (b) Zn(0.40 ML)/Cu(997) at 373 K under (CO_2 + H_2) gas mixture (total pressure of 1.2 mbar) as a function of elapsed time. CO_2 gas (0.8 mbar) was introduced in the gas cell at t = 0 s, and then H_2 gas (0.4 mbar) was added.

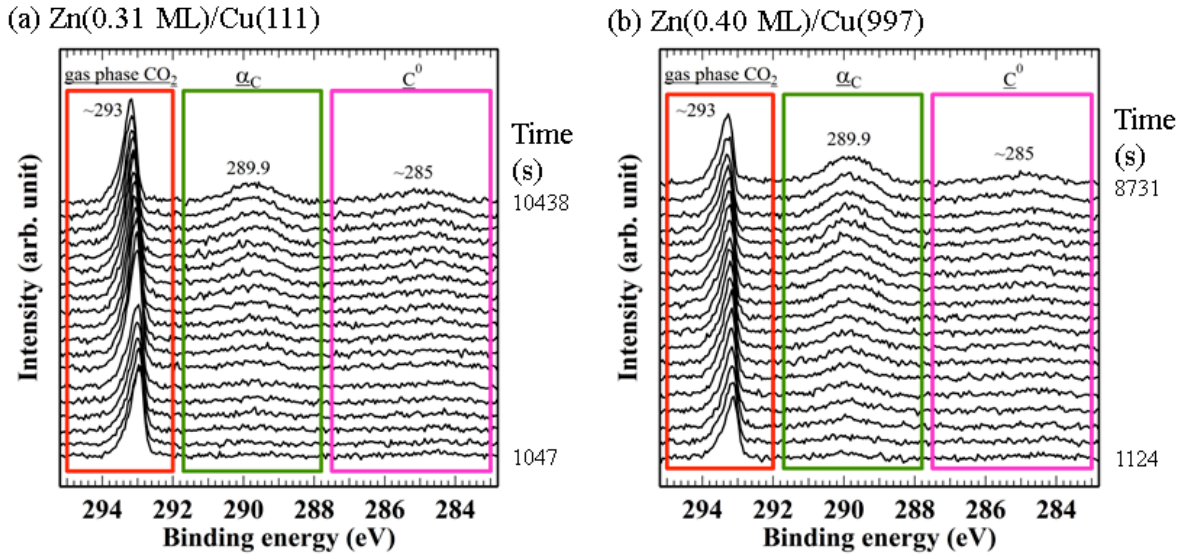

Figure 1 A series of C 1s AP-XPS spectra of (a) Zn(0.31 ML)/Cu(111) and (b) Zn(0.40 ML)/Cu(997) at 373 K under (CO_2 + H_2) gas mixture (total pressure of 1.2 mbar) as a function of elapsed time. The photon energy was 630 eV. CO_2 gas (0.8 mbar) was introduced in the gas cell at t = 0 s, and then H_2 gas (0.4 mbar) was added to the gas cell.

Peaks at 293 eV and 285 eV are assigned to gas-phase CO_2 and neutral carbon species (C^0), respectively. The peak at 289.9 eV (α_c in Fig. 1) is assigned to carbonate (CO_3) formed from CO_2 by following reactions,

$CO_2 \rightarrow CO(gas) + O$, (1)

$O + CO_2 \rightarrow CO_3$. (2)

Hydrogenation products such as formate (HCOO) and methoxy (CH_3O) species were not detected under the present reaction conditions.

As seen in Fig. 1, the formation of CO_3 is faster on Zn-Cu(997) than on Zn-Cu(111), indicating a stepped surface is more reactive than a flat surface. Figure 2 shows CO_3 coverages as a function of elapsed reaction time. From linear fitting of the uptake curves, (initial) CO_3 formation rates were estimated to be 9.1×10^{-6} ML/s on Zn-Cu(111) and 1.8×10^{-5} ML/s on Zn-Cu(997), respectively. These values correspond to very small CO_3 formation probabilities per one CO_2 collision: 4.9×10^{-11} (9.4×10^{-11}) on Zn-Cu(111) (Zn-Cu(997)). Such rare reaction can be detectable only in the near-ambient condition using the *operand* techniques. Note that the estimated CO_3 formation probabilities are similar to the dissociation probability of CO_2 on Cu(110) at 450 K (~ 10^{-11} per collision) [7], indicating that the CO_2 dissociation (1) is a rate-limiting step for the CO_3 formation.

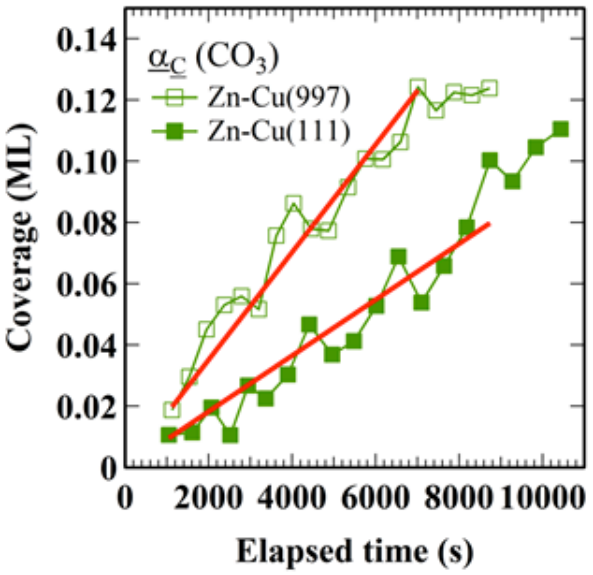

Figure 2 CO_3 coverage on Zn-Cu(111) (■) and Zn-Cu(997) (□) as a function of elapsed time. Reaction rates were roughly estimated from linear fitting of the uptake curves.

REFERENCES

[1] A. Dibenedetto, A. Angelini, P. Stufano, "Use of carbon dioxide as feedstock for chemicals and fuels: homogeneous and heterogeneous catalysis" J. Chem. Technol. Biotechnol. **89**, 334-353 (2014).

[2] M. Aresta, "Carbon dioxide as chemical feedstock" (Wiley-VCH, Weinheim, 2010).

[3] G. A. Olah, A. Goeppert, G. K. Surya Prakash, "Beyond oil and gas: The methanol economy" (Wiley-VCH, Weinheim, 2009).

[4] J. Nakamura, Y. Choi, and T. Fujitani, "On the issue of the active site and the role of ZnO in Cu/ZnO methanol synthesis catalysts" Top. Catal. **22**, 277-285 (2003).

[5] M. Behrens et al., "The Active Site of Methanol Synthesis over $Cu/ZnO/Al_2O_3$ Industrial Catalysts" Science **336**, 893-897 (2012).

[6] T. Koitaya, S. Yamamoto, Y. Shiozawa, K. Takeuchi, R.Y. Liu, K. Mukai, S. Yoshimoto, K. Akikubo, I. Matsuda, and J. Yoshinobu "Real-time observation of reaction processes of CO_2 on Cu(997) by ambient-pressure X-ray photoelectron spectroscopy" Top. Catal. **59**, 526-531 (2016).

[7] J. Nakamura, J. A. Rodriguez and C. T. Campbell "Does CO_2 dissociatively adsorb on Cu surfaces?" J. Phys.: Condens. Matter **1**, SB149-SB160 (1989).

REVEALING ROOM-TEMPERATURE FERROMAGNETISM OF $ZnSnAs_2$: Mn THIN FILMS BY ATOMIC AND MAGNETIC STRUCTURE ANALYSIS BASED ON PHOTOELECTRON HOLOGRAPHY AND SITE-SELECTIVE XPS MEASUREMENTS

Naotaka Uchitomi[1], Masaki Ogo[1], Yusuke Hashimoto[2], Mihee Lee[2], Shun Fukami[2], Daichi Tsujikawa[2], Taisuke Yoshida[2], Hiroyuki Matsuda[2], Munetaka Taguchi[2], and Hiroshi Daimon[2]

[1]*Department of Electrical Engineering, Nagaoka University of Technology, Niigata, Japan*

[2]*Graduate School of Materials Science Laboratory, Nara Institute of Science and Technology*

During the last two decades, III-V based diluted magnetic semiconductors (DMSs), as well as recently developed ferromagnetic metals, have attracted much attention for use in spintronic devices and as candidates for beyond-CMOS technology. In particularly, GaMnAs has been extensively studied from experimental and theoretical points of view. This is because of well lattice-matching with GaAs substrates and a high Curie temperature of more than 100 K [1-4]. Thus, GaMnAs is a promising candidate for producing semiconductor spintronic devices. On the other hands, II-IV-V2 chalcopyrite semiconductors such as $CdGeP_2$[5], $CdGeAs_2$[6] and $ZnSnAs_2$[7-8] are alternative ferromagnetic semiconductor, which have been shown to become ferromagnetic by Mn doping, and have Curie temperatures higher than 300 K. In particularly, a bulk-type Mn doped $ZnSnAs_2$ crystal has been experimentally shown to be ferromagnetic at a high Curie temperature [7]. The magnetic Mn ion, which occupies the cation IV site in host chalcopyrite or zinc-blende (sphalerite) structures, has a local spin moment and acts as an acceptor at the same time.

Very recently, $ZnSnAs_2$: Mn thin films have been epitaxially grown on InP (001) without any secondary phases, and have shown room-temperature ferromagnetism [8-10]. $ZnSnAs_2$ would be regarded as a “vertical GaAs” to some extent experimentally and theoretically, consisting of two interposing zinc-blende lattices, while permitting a high degree of Mn incorporation because Mn^{2+} ions may easily substitute on the group II Zn sites. The $ZnSnAs_2$ thin films grown by molecular beam epitaxy (MBE) tend to show zinc-blende structure rather than chalcopyrite structure, which is analogous to the GaAs zinc-blende structure with Ga atoms being randomly replaced with either a Zn or Sn atom. As a results, the ternary compound $ZnSnAs_2$ grown by MBE is referred to as zinc-blende $ZnSnAs_2$. On the basis of the present results, this material has the potential to produce InP-based spintronic devices, for which the lattice-matched III-V semiconductors InGaAs and InAlAs are expected to make possible magnetic quantum-well structures. However, the state of research and development of ferromagnetic II-IV-V2 chalcopyrite semiconductors is still under debate, and basic information is still not available on the parameters needed for spintronic device application.

In 2015A beam-time, we have measured the photoelectron diffraction of Mn doped $ZnSnAs_2$. 2D-PES measurements were performed at the free port of BL07LSU in SPring-8. The DELMA combined with an energy analyser (VG SCIENTA R4000) was used to obtain two dimensional photoelectron intensity distribution (2D-PIAD) patterns and also conventional angle integrated core-level x-ray photoemission spectra. DELMA is a photoelectron spectroscopy device that has the photoelectron emission microscope function, spatial resolution about 100 μm now, which allows us to measure two dimensional photoelectron intensity angular distribution (2D-PIAD) of the individual small regions in the sample microscopically. Figure 1 shows a measured 2D-PIAD patterns of doped Mn in $ZnSnAs_2$. Unfortunately, no visible PAID pattern of dopant Mn site is detected, probably due

to the low doping concentration of Mn. However, as shown in Fig.2, we observed the angle integrated XPS spectrum of Mn *2p*, in which the spectral shape is quite similar to Mn^{2+} spectrum such as MnO[11]. This suggest that the valency of Mn atom is 2+.

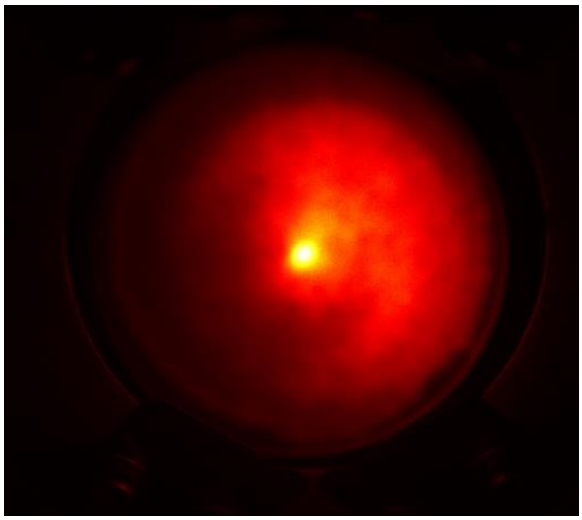

Figure 1: 2D-PIAD pattern of Mn *2p*

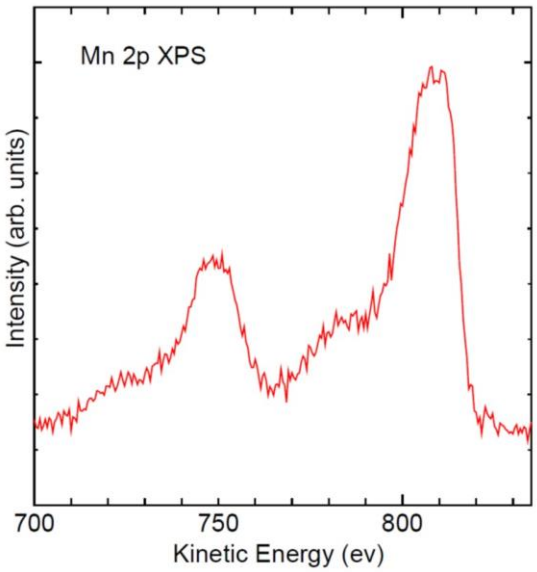

Figure 2: Mn *2p* XPS spectrum

ACKNOWLEDGMENT

This work was supported by KAKENHI (Grants No. 26105001).

REFERENCES

[1] H. Ohno, Science **281**, 951 (1998)..
[2] T. Jungwirth, *et al*., Rev. Mod. Phys. **78**, 809 (2006).
[3] T. Dietl, H. Oono, F. Matsukura, Phys. Rev. B **63**, 195205 (2001).
[4] S. Sato, M. A. Osman, Y. Jinbo, N. Uchitomi, Appl. Surf. Sci. **242**, 134 (2005).
[5] G. A. Medvedkin, *et al.*, Jpn. J. Appl. Phys. **39**, L949 (2000).
[6] R. Demin, *et al*., J. Magn. Magn. Matter. **290-291**, 1379 (2005).
[7] S. Choi, *et al*., Solid State Commun. 122, 165 (2002).
[8] J.T. Asubar, Y. Jinbo, N. Uchitomi, J. Cryst. Growth **311**, 929 (2009).
[9] N. Uchitomi, H. Oomae, J. T. Asubar, H. Endo, Y. Jinbo, Jpn. J. Appl. Phys. **50**, 05FB02 (2011).
[10] H. Oomae, J. T. Asubar, Y. Jinbo, N. Uchitomi, Jpn. J. Appl. Phys. **50**, 01BE12 (2011).
[11] M. Taguchi *et al.*, J. Phys. Soc. Jpn. **66**, 247 (1997).

Co 2*p*-3*d*-2*p* RESONANT X-RAY EMISSION SPECTRUM OF $LaCoO_3$ BELOW ROOM TEMPERATURE

Yukihiro Taguchi,[1] Kengo Kashiwagi,[1] Masakazu Hamada,[1] Shuichi Kawamata,[1] Takayuki Uozumi,[1] Kojiro Mimura,[1] Atsushi Hariki,[2] Jun Miyawaki,[3] and Yoshihisa Harada[3]

[1]*Graduate School of Engineering, Osaka Prefecture University,*

[2]*Institute of Physics, Academy of Sciences of the Czech Republic,*

[3]*Synchrotron Radiation Laboratory, The Institute for Solid State Physics, The University of Tokyo*

The ground state of Co ions in $LaCoO_3$ is a nonmagnetic low-spin (LS, t_{2g}^6) state with S=0. With increasing temperature $LaCoO_3$ undergoes a gradual non-to-paramagnetic transition and exhibits a maximum around 100 K in the χ-T curve. Since a model where a high-spin (HS, $t_{2g}^4 e_g^2$) state with S=2 is uniformly excited gives much higher magnetic susceptibility than that observed in the experiments, proposed has been a model where an intermediate-spin (IS, $t_{2g}^5 e_g^1$) state with S=1 is excited below room temperature [1]. So far extensive studies have been carried out to identify the excited spin-state involved in the transition of $LaCoO_3$ around 100 K. Some studies support the LS-to-HS model [2], others the LS-to-IS or LS-to-IS and HS model [1]. It is expected that the different spin-states give different electronic-structure from each other, because the different spin-states arise from different configurations of the Co 3*d* electrons. However, x-ray absorption and photoemission spectra of $LaCoO_3$ do not show significant temperature dependence below room temperature [1,2]. Since it is expected that the *dd* excitations of the Co 3*d* electrons are sensitive to the change in the spin state of $LaCoO_3$, we performed Co 2*p*-3*d*-2*p* resonant x-ray emission spectroscopy, or resonant inelastic x-ray scattering experiment for $LaCoO_3$ to observe the change in the *dd* excitations through the 100-K transition. Although the difference between the spectra at 40 and 300 K due to the spin-state transition was clearly observed, it was not possible to identify the excited spin-state definitely because of low energy-resolution of the spectra and rather large contribution from fluorescent-like feature which shows spectral shape like that in the Co 3*d*-2*p* normal emission [3]. The soft x-ray emission spectrometer and the light source have been remarkably improved in recent years [4]. We have performed the same experiment with the new experimental setup.

The Co 2*p*-3*d*-2*p* x-ray emission experiments were carried out by using the soft x-ray emission spectrometer constructed at the BL07LSU beamline of SPring-8 [4]. The overall energy resolution was 0.34 eV. Sample used was single-crystalline $LaCoO_3$ and was fractured *in situ* before the experiments. The sample temperature was set from 40 to 300 K.

Figure 1 shows the Co 2*p*-3*d*-2*p* resonant x-ray emission spectra for $LaCoO_3$ at 40 (blue curve) and 300 K (red) in the depolarized configuration [5]. The excitation energy was set at 4.5 eV higher than the Co L_3 absorption peak to separate the fluorescent-like feature from the electronic-Raman feature. The former is seen from around 4 eV to higher Raman-shift side and the latter below 4 eV in Fig. 1. It was difficult in our previous experiment to take the spectrum with sufficient signal-to-noise ratio for excitation energies in the region where photoabsorption signal is rather weak. As was observed in the previous study, the elastic scattering at 0 eV is seen in the 300-K spectrum, whereas it is absent in the 40-K spectrum. This indicates that the spin state(s) other than the LS state are thermally excited at 300 K whereas almost all Co ions at 40 K is in the LS state. The elastic scattering is forbidden for the totally symmetric LS ($^1A_1$) state in the depolarized configuration [5]. In addition, the peak of fluorescent-like feature around 7 eV is somewhat broadened with increasing temperature. The fluorescent-like emission is nearly independent of the photoexcited electron. In other words, it goes through the intermediate state similar to the final state of the Co 2*p* x-ray photoemission. The Co 2*p* photoemission is broadened with increasing temperature because the thermally excited spin-state opens up the non-local screening channel [6]. The increase in population of the IS or HS states may be responsible for the temperature-induced broadening of the fluorescent-like feature.

Two Raman peaks are seen at 0.75 and 1.35 eV in the 40-K spectrum. These are in agreement with two peaks at 0.8 and 1.5 eV in the calculated spectrum for $LaCoO_3$ in the LS state by using a *dp* model simulating Co 3*d* and O 2*p* orbitals by means of a dynamical mean-field approach under the perovskite crystal structure [7]. The calculation has been carried out for the depolarized configuration with the excitation energies corresponding to distinctive features in the Co L_3 absorption of $LaCoO_3$. It shows that the positions of the Raman peaks below 3 eV changes little by varying the excitation energy, although the relative intensity among the peaks changes significantly. The calculated spectrum for $LaCoO_3$ in the HS state exhibits two peaks at 0 and 1.2 eV. These also agree with the observed peaks at 0 and around 1 eV in the 300-K spectrum. The calculation for the HS state predicts that a feature resulting from the non-local screening appears between the two peaks. A shoulder at 0.6 eV in the 300-K spectrum may be related to the predicted feature.

To summarize, we have observed the change in the Co 2*p*-3*d*-2*p* resonant x-ray emission spectrum of $LaCoO_3$ through the gradual magnetic transition below room temperature. The results are consistent with the low-to-high spin model for the transition.

REFERENCES

[1] T. Saitoh *et al*., *Phys. Rev. B* **55** (1997) 4257.
[2] M. W. Haverkort *et al., Phys. Rev. Lett.* **97** (2006) 176405.
[3] Y. Taguchi *et al., Surf. Rev. Lett.* **9** (2002) 871.
[4] Y. Harada *et al., Rev. Sci. Instrum.* **83** (2012) 013116.
[5] M. Matsubara *et al., J. Phys. Soc. Jpn.* **69** (2000) 1558.
[6] A. Hariki *et al., J. Phys. Soc. Jpn.* **84** (2015) 073706.
[7] A. Hariki, A. Yamanaka and T. Uozumi, unpublished.

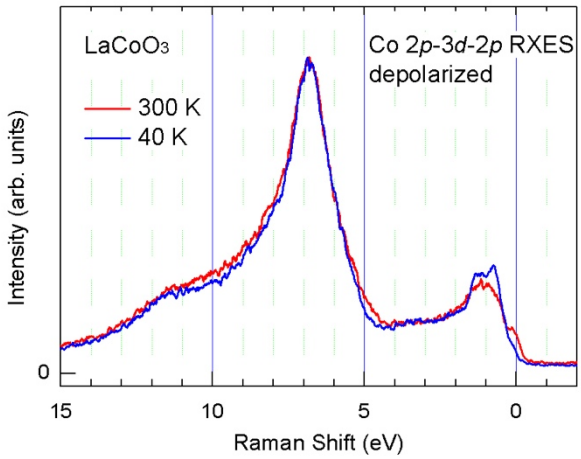

Fig. 1. Co 2*p*-3*d*-2*p* resonant x-ray emission spectra for $LaCoO_3$ in the depolarized configuration at 40 (blue curve) and 300 K (red).

Improvement of *operando* cell of $LiCoO_2$ cathode for the Co 2*p* soft x-ray emission spectroscopy

Daisuke Asakura[1], Eiji Hosono[1], Hideharu Niwa[2,3], Hisao Kiuchi[4], Jun Miyawaki[2,3], and Yoshihisa Harada[2,3]

[1]*Research Institute for Energy Conservation, National Institute of Advanced Industrial Science and Technology*

[2]*Institute for Solid State Physics, The University of Tokyo*

[3]*Synchrotron Radiation Research Organization, The University of Tokyo*

[4]*Department of Applied Chemistry, The University of Tokyo*

To understand the electrochemical performances of electrode materials for Li-ion batteries (LIBs), characterizations of the chemical and physical properties are of particular importance. Electron spectroscopy at synchrotron facilities, such as X-ray absorption, is the most promising technique to reveal the electronic structure. Recently, electronic-structure analyses for the electrode materials using soft x-ray spectroscopy have been highly attractive because the 3*d* orbital of transition metals can be clarified directly.

We have successfully performed *operando* soft x-ray emission spectroscopy (XES) for $LiMn_2O_4$[1]. The *operando* cell consisted of the $LiMn_2O_4$ thin-film cathode, a Li-metal counter electrode and an organic electrolyte solution. The *operando* XES experiments were carried out using ultrahigh-resolution x-ray emission spectrometer, HORNET[2] at BL07LSU of SPring-8.

Then, we have been applying the same method to other typical electrode materials. We have tried to make $LiCoO_2$ thin-film cathode for Co 2*p* *operando* XES. However, the results of cyclic voltammetry and XES have indicated insufficient charge-discharge reactions possibly due to a high resistivity in the *operando* cell[3]. In order to reduce the resistivity, we slightly modified the thin-film structure: Si_3N_4 (150 nm)/Al_2O_3 (5 nm)/Ti (20 nm)/Au (15 nm)/$LiCoO_2$ from the vacuum side to electrolyte side. The Al_2O_3 layer and Ti/Au multilayer were fabricated by RF sputtering and electron-beam deposition, respectively. The $LiCoO_2$ layer was fabricated by sol-gel method. The thickness of $LiCoO_2$ thin-film was estimated to be about 50 nm from a result of scanning electron microscopy. Although the processes are similar to those for previous case, the 15-nm thick Au layer and a shorter heating time for fabrication of $LiCoO_2$ are effective to maintain a low resistivity (~10 Ω) on the Au current collector. Figure 1 shows the cyclic voltammetry (CV) curves of the $LiCoO_2$ thin film with the *operando* cell. The cathodic and anodic peaks evidence a charge-discharge reaction of $LiCoO_2$[4].

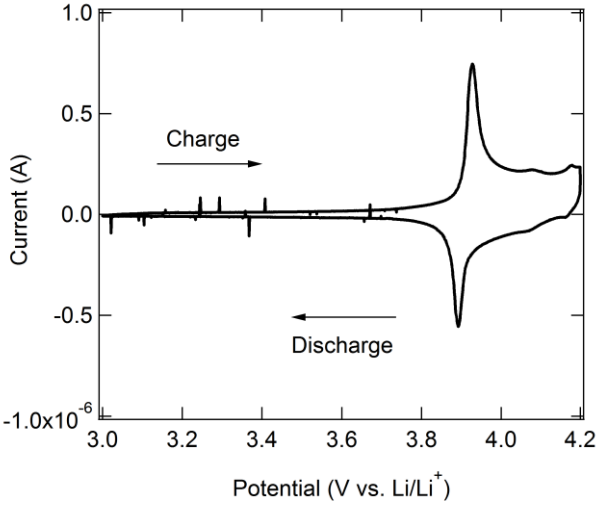

Fig. 1. CV curves of $LiCoO_2$ thin film with *operando* cell. The scan speed was 0.5 mV/s.

However, unfortunately, the thin-film

window was broken at the vacuum pumping. Instead, Co 2*p* *ex situ* XES measurements for the $LiCoO_2$ thin films were carried out. Figure 2 shows the *ex situ* XES results in the case of excitation energy of 779.4 eV. In going to the charged state, the XES profile slightly changed compared to the initial state, while the XES for the discharged state was almost the same as that for the charged state. Similar tendencies were found for the results with the other excitation energies. Most likely, these results would be due to the *ex situ* condition. For the $LiCoO_2$ thin film having a layered structure, the charged state should be unstable unlike spinel-type $LiMn_2O_4$ and olivine-type $LiFePO_4$. Now, we are making the window area smaller to avoid the break of the window. In the near future, we will be able to perform the *operando* XES using the improved $LiCoO_2$ thin film.

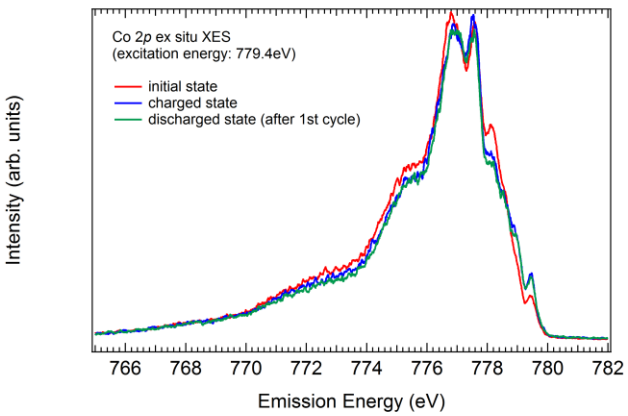

Fig. 2. Co 2*p* *ex situ* XES for the $LiCoO_2$ thin film. The samples were taken from beaker cells after the charge/discharge treatments and prepared under an *ex situ* condition.

References

[1] D. Asakura *et al*., Electrochem. Commun. **50**, 93 (2015).
[2] Y. Harada *et al*., Rev. Sci. Instrum. **83**, 013116 (2012).
[3] D. Asakura *et al*., ISSP Activity Report of Synchrotron Radiation Laboratory 2014.
[4] D. Takamatsu *et al*., Angew. Chem. Int. Ed. **51**, 11597 (2012).

Magnetic Circular Dichroism in RIXS of weak ferromagnet α-Fe_2O_3

J. Miyawaki[1,2], S. Suga[3], H. Fujiwara[4], H. Niwa[1,2], H. Kiuchi[5] and Y. Harada[1,2]

[1]*The Institute for Solid State Physics (ISSP), The University of Tokyo, Japan,*
[2]*Synchrotron Radiation Research Organization, The University of Tokyo, Japan,*
[3]*Institute of Scientific & Industrial Research, Osaka University, Osaka, Japan,*
[4]*Graduate School of Engineering Science, Osaka University, Osaka, Japan,*
[5]*Department of Applied Chemistry, The University of Tokyo*

Typical weak ferromagnetic material, α-Fe_2O_3 has the corundum structure and is an antiferromagnet: Below the Morin temperature (T_M), spin moments align along [111] direction of the rhombohedral lattice, while above T_M the (spin) moments show spin reorientation to the basal plane and are slightly canted due to Dzyaloshinskii-Moriya interaction, resulting in weak ferromagnetism. In this study, magnetic circular dichroism (MCD) in Fe *L*-edge soft x-ray resonant inelastic x-ray scattering (SX-RIXS) of α-Fe_2O_3(111) single crystal was measured at room temperature (RT) to identify the electronic structure and mechanism inducing weak ferromagnetism.

SX-RIXS experiments were carried out at ultrahigh-resolution soft x-ray emission spectroscopy station at BL07LSU in SPring-8 [1,2] where a measurement system for MCD in SX-RIXS has been developed. Magnetic fields of ~0.25 T can be applied to a sample placed at the center of the magnetic poles. The magnet can be rotated around the axis perpendicular to the x-ray scattering plane, and SX-RIXS can be obtained by applying the magnetic field parallel and 45 degrees to the incident X-ray. A dedicated sample stage was designed to be as small as possible to allow RIXS measurements at arbitrary incident angles by rotating the stage between the magnetic poles. MCD in RIXS was measured at RT with grazing incidence (10 degree from the sample surface). In order to investigate the crystal orientation dependence, two different azimuthal angles in the (111) plane were chosen: the incidenty x-ray was parallel and perpendicular to the axis of the rhombohedral lattice. The magnetic field was always set parallel to the incident x-ray.

Figure 1 shows (a) Fe $L_{3,2}$-edge x-ray absorption spectroscopy (XAS), (b) excitation energy dependence of SX-RIXS and (c) MCD in RIXS of α-Fe_2O_3. The XAS spectrum agrees very well with previous experimental results and calculations [3,4]. Figure 1(b) exhibits inelastic components in RIXS at 1–6 eV loss energy, which are assigned to *dd* transition ($^6A_{1g}\rightarrow{}^4T_{1g}$ and $^6A_{1g}\rightarrow{}^4T_{2g}$), spin flip and charge transfer transition according to previous optical absorption experiments and calculations [5,6]. Selected MCD in RIXS at 1–2 eV are shown in Fig. 1(c). MCD in RIXS was not at all detected for the main peak (5) excitation of L_3-edge XAS and was observed only at 1.8 eV loss energy and for the excitations above $h\nu = 713.25$ eV, where charge transfer transition contributes substantially. Since any discernible MCD was not recognized in XAS, the observed MCD in RIXS can be safely attributed to the RIXS process and was confirmed by *ab-initio* multiplet calculations. Moreover, with the incident x-ray parallel to the axis of the rhombohedral lattice, the MCD in RIXS was not observed at any excitation energies, thus exhibiting the crystal orientation dependence. These results suggest that the intermediate states in RIXS excited to the charge transfer transition induce anisotropic MCD in RIXS, indicating the importance of the coordination of oxygen atoms in the magnetic order.

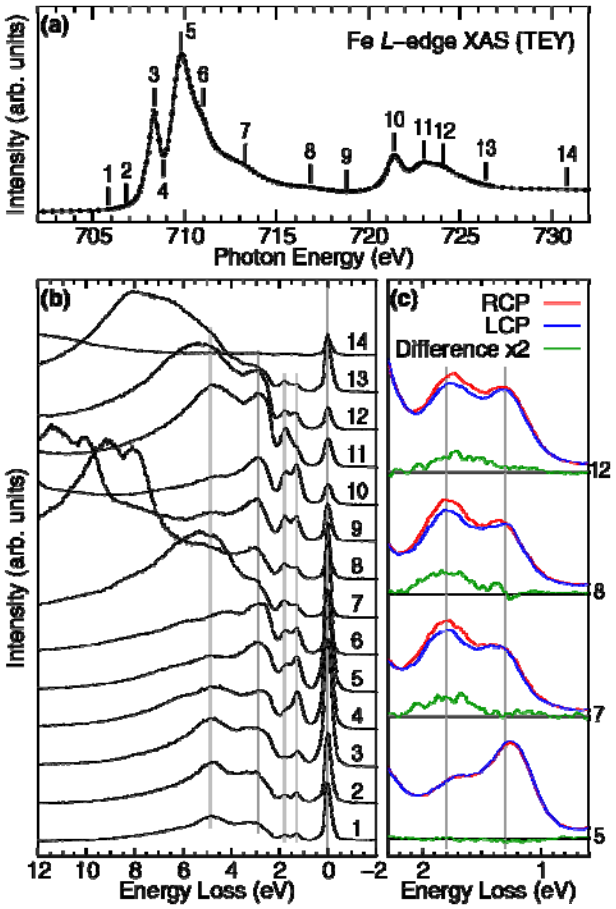

Fig. 1 Fe *L*-edge XAS and RIXS with the incident x-ray perpendicular to the axis of the rhombohedral lattice. (a) Fe $L_{3,2}$-edge XAS measured at RT by total electron yield (TEY) mode. (b) The excitation energy dependence of Fe *L*-edge RIXS. (c) Corresponding MCD in RIXS. Numbers labeled on RIXS indicate excitation energies shown in (a).

REFERENCES

[1] Y. Harada *et al.*, *Rev. Sci. Instrum.* **83**, 013116 (2012).
[2] S. Yamamoto *et al.*, *J. Synchrotron Rad.* **21**, 352 (2014).
[3] P. Kuiper *et al.*, *Phys. Rev. Lett.* **70**, 1549 (1993)
[4] H. Kurata *et al.*, *J. Electron Microsc.* **47** 293 (1998).
[5] L. A. Marusak *et al.*, *J. Phys. Chem. Solids* **41**, 981 (1980)
[6] A. I. Galuza *et al.*, *Low Temp. Phys.* **24**, 716 (1998).

ANALYSIS OF DOPANT-SITE IN BORON DOPED DIAMOND BY USING PHOTOELECTRON HOLOGRAPHY

Yukako KATO*

Advanced Power Electronics Research Center, Advanced Industrial Science and Technology

Semiconducting diamond has attracted considerable attention as a more advanced-generation material for power devices owing to its ability to perform with high breakdown characteristics and high carrier mobility in a high-temperature, high-voltage environment. The latest progress of development of diamond power devices is remarkable. For example, the reported diamond Schottky barrier diode (SBD) worked stable at temperatures above 200°C[1]. On the other hand, high switching performance under high temperature was shown[2]. However, there is no achievement report about the high performance diamond power device based on the ideal material character.

In this study, we will discuss about "active dopant-site in diamond", because it is known that the dopant concentration is not same as carrier concentration [3, 4]. One of reasons under discussion is relationship between contribution to device performance and dopant site. We assumed that dopant at substitutional site is worked as accepter. However, there is no data for discuss about existence of other dopant site.

We analyzed an epitaxial boron-doped diamond grown by plasma-assisted CVD method. The substrate was a type-Ib single-crystal diamond (001) plate provided by Sumitomo Electric Industries, Ltd, Japan. The substrate size and thickness were 3 mm × 3 mm and 0.5 mm, respectively. The boron concentration was controlled by changing the B/C ratio of the source gas with trimethylboron (TMB) and methane (CH4) concentration. In this study, The B/C ratios and CH4 concentrations was 2000 ppm and 0.5%, respectively. The film thickness was approximately to 1 μm. Boron atomic concentration, $3\times10^{20}/cm^3$, is estimated from SIMS. By the Hall effect measurement at room temperature, hall coefficient and hall mobility are $3.63\times10^{-4}[cm^3/C]$ and $3.85\times10^{-1}[cm^2/Vs]$, respectively.

For active-site analysis, photoelectron diffraction pattern has been expected to be a powerful tool for visualizing local atomic structures around a photoelectron emitter atom[5, 6]. Photoelectron diffraction pattern was observed by using Display-type Ellipsoidal Mesh Analyzer (DELMA) installed at free-port in BL07LSU. A photoelectron diffraction pattern caused by a scatterer atom has a strong forward focusing peak (FFP) and ring patterns around it. The scatterer atom located farther away from the emitter atom forms finer ring patterns. The FFP indicates the direction of the scatterer atom. The fineness of ring patterns indicates the atomic distance. Thus, the photoelectron hologram provides an image around a photoelectron emitter atomic site without requiring any initial model or phase information. It is possible to assign not only the bulk structure but also the surface structure and the local impurity structure of the crystal. Therefore, it is a powerful tool for the analysis of atomic structures. Up to now, much effort has been devoted to the study of atomic resolution holography using photoelectron [7, 8].

Figure 1a is C1s photoelectron diffraction pattern of boron doped diamond at kinetic energy of 600 eV. A comparison of the observation (fig. 1a) with the computed results (fig. 1b) shows good agreement. Figure 1c is schematic image of diamond unit cell for explain about angles and distances between emitter and scatterer. Red atom is one site of emitter 1. Other colored atoms are scatterer. Emitter and scatterer which are superimposed in Fig.1b as same colored circle. This calculated photoelectron diffraction pattern was simulated by TMSP with hemispherical atomic cluster shown in fig.1d. TMSP is a simulation program for photoelectron hologram developed by Dr. T. Matsushita[9]. Hemispherical atomic cluster's size radius is about 7Å.

Two-dimensional photoelectron image of B1s is not able to be obtained because S/N may be too poor to analysis setting parameter.

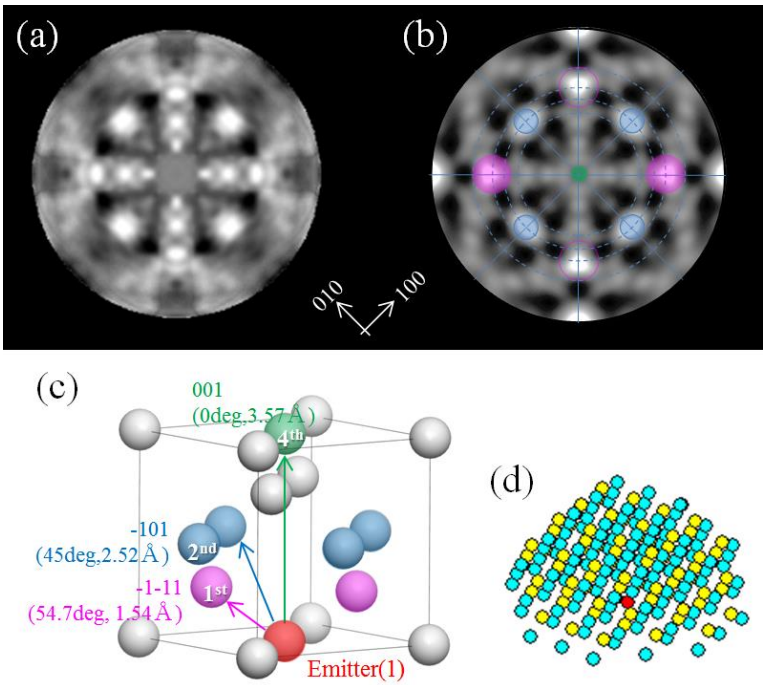

Fig. 1) Experimental data and calculated data with schematic atomic structure.

(a) Observed C1s photoelectron diffraction pattern. Kinetic energy is set to 600 eV.

(b) Calculated C1s photoelectron diffraction pattern. Superimposed circles mean FFP of photoelectron of each atomic site shown in fig. 1c.

(c) Schematic image of diamond unit cell for explain about angles and distances between emitter and scatterer. Red atom is one site of emitter (1). Other colored atoms are scatterer. Scatterer are superimposed in Fig.1b as same colored circle.

(d) Atomic cluster of diamond (001) for the hologram calculation. Red circle is emitter and other circles are scatterer.

ACKNOWLEDGMENT

This work was supported by KAKENHI (Grants No. 15H01056).

REFERENCES

[1] H. Umezawa, K. Ikeda, R. Kumaresan, S. Shikata, High Temperature Characteristics of Diamond SBDs. Mater. Sci. Forum, 645–648 (2010) 1231–1234.

[2] H. Umezawa, S.-i. Shikata, T. Funaki, Diamond Schottky barrier diode for high-temperature, high-power, and fast switching applications. Japanese Journal of Applied Physics, 53 (2014) 05FP06.

[3] W. Gajewski, P. Achatz, O.A. Williams, K. Haenen, E. Bustarret, M. Stutzmann, J.A. Garrido, Electronic and optical properties of boron-doped nanocrystalline diamond films. Physical Review B, 79 (2009) 045206.

[4] J.W. Ager III, M.D. Drory, Quantitative measurement of residual biaxial stress by Raman spectroscopy in diamond grown on a Ti alloy by chemical vapor deposition. Phys. Rev. B, 48 (1993) 2601–2607.

[5] T. Matsushita, F. Matsui, K. Goto, T. Matsumoto, H. Daimon, Element Assignment for Three-Dimensional Atomic Imaging by Photoelectron Holography. Journal of the Physical Society of Japan, 82 (2013) 114005.

[6] H. Daimon, Direct Imaging of Atomic Arrangement by Photoelectron Holography. e-Journal of Surface Science and Nanotechnology, 10 (2012) 169-174.

[7] F. Matsui, T. Matsushita, H. Daimon, Photoelectron Diffraction and Holographic Reconstruction of Graphite. Journal of the Physical Society of Japan, 81 (2012) 114604.

[8] M.V. Kuznetsov, I.I. Ogorodnikov, A.S. Vorokh, A.S. Rasinkin, A.N. Titov, Characterization of 1T-TiSe2 surface by means of STM and XPD experiments and model calculations. Surface Science, 606 (2012) 1760-1770.

[9] T. Matsushita, F. Matsui, H. Daimon, K. Hayashi, Photoelectron holography with improved image reconstruction. Journal of Electron Spectroscopy and Related Phenomena, 178–179 (2010) 195-220.

Monitoring the ferroelectric instability of BaTiO3 by RIXS

[1]Fatale Sara, [1]Moser Simon and [1]Grioni Marco
[1] *Ecole Polytechnique Federale de Lausanne*

Purpose of the experiment and summary of the results:

Barium titanate ($BaTiO_3$) is a well-known, technologically important ferroelectric material. It exhibits a high transition temperature, $T_C \sim 130$ °C and various structural phases as a function of temperature [1-2].

Despite the enormous applications of this compound, the microscopic origin of the ferroelectricity is complex, calling for combination of theoretical models.

We decided to investigate the role of the electron-phonon coupling across the ferroelectric instability by means of temperature dependent RIXS measurements.

We could identify the spectral signature of phonon excitations at the Ti-L_3 absorption threshold and found that they persist along all the structural phase transitions occurring in the material.

Experimental method and key experimental data:

Ti L_3-edge RIXS data have been acquired at Hornet end station of BL07LSU at SPring8. Data have been collected with: π-polarized light, a fixed 90° scattering angle and an incidence angle of 55°, corresponding to a transferred momentum 10° off from the ferroelectric axis.

Close to the elastic response, phonon excitations can be enhanced by tuning the incoming photon energy to the eg absorption peak (Fig1.a). The phonon response is present for all temperature conditions, meaning different structural phases: from rombohedral to cubic.

Conclusion, examination and reference list:

A Franck-Condon model has been used to simulate the data [3].

A quite good agreement has been found for a phonon energy of $h\omega = 65$ meV (Fig1.c).

Phonon modes of energy around $h\omega \approx 60$ meV have been already measured in this compound by means of Raman experiments [4-6].

The Franck-Condon model allows us to estimate the electron-coupling constant and compare it to the one obtained on a similar compound (TiO2), already investigated by us [7-8].

REFERENCES:

[1] C.A. Randall et al, Cross Materials Research Institute The Pennsylvania State University University Park, PA 16802 USA
[2] R.E. Cohen and H. Krakauer, Phys. Rev. B 42, 10 (1990)
[3] L. J. P. Ament et al., EPL (95) 27008 (2011)
[4] G.A. Barbosa et al., Solid State Comm. 11, 1053-1055 (1972)
[5] M.P. Fontana et al., Solid State Comm. 10, 1-4 (1972)
[6] M. Lambert et al., Solid State Comm. 7, 305-308 (1969)
[7] S. Moser et al., Phys. Rev. Lett. 110, 196403 (2013)
[8] S. Moser et al. Phys. Rev. Lett. 115, 096404 (2015)

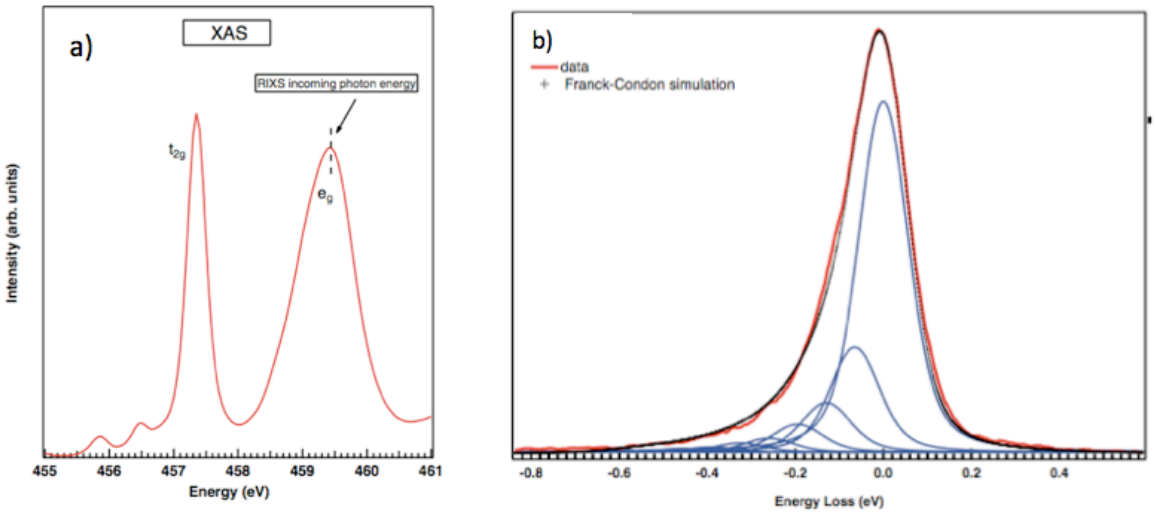

a) XAS spectrum at room temperature. Dashed vertical line indicates the energy of the incoming photons for RIXS measurements.
b) Franck-Condon simulation.

DEVELOPMENT OF AMBIENT PRESSURE ANGLE RESOLVED ULTRA-HIGH RESOLUTION RIXS SYSTEM

Yoshihisa Harada*, Jun Miyawaki, Hideharu Niwa, Hisao Kiuchi,
Kosuke Yamazoe, Takanobu Inoue, Yitao Cui
Synchrotron Radiation Laboratory, The Institute for Solid State Physics, The University of Tokyo

We have constructed and developed an ultra-high resolution soft X-ray emission (or resonant inelastic X-ray scattering = RIXS) spectrometer with its energy resolution E/ΔE > 8000 optimized in the energy range from 350 eV to 750 eV as an endstation for the University of Tokyo outstation beamline BL07LSU in SPring-8. The RIXS station is dedicated for soft X-ray emission spectroscopy under various environmental conditions (gases, liquids and solids). In 2015, three major upgrades of the station has almost been accomplished, i.e. differential pumping system for windowless atmospheric pressure experiments, installation of a spectrometer rotation system for angle resolved RIXS experiments, and installation of ultra-precise low slope-error post-focusing mirror to realize 1μm-level focusing of soft X-rays. Commissioning exams of the angle resolved RIXS will be implemented in the first half of 2016 cycle and will be open to users in the second half.

Figure 1 shows the differential pumping system for real ambient pressure RIXS experiments. For the incident beam we have succeeded in the real ambient pressure at sample position because we can put small (1-2mm diameter) apertures that do not intersect the low emittance beam, while for the emission we should overcome a lot of difficulties in order to collect divergent fluorescence and/or RIXS signals. Finally we have succeeded in a quasi-ambient (ca. 0.5 bar) pressure O K-edge RIXS experiments on SiO_2, which is shown in Fig. 2.

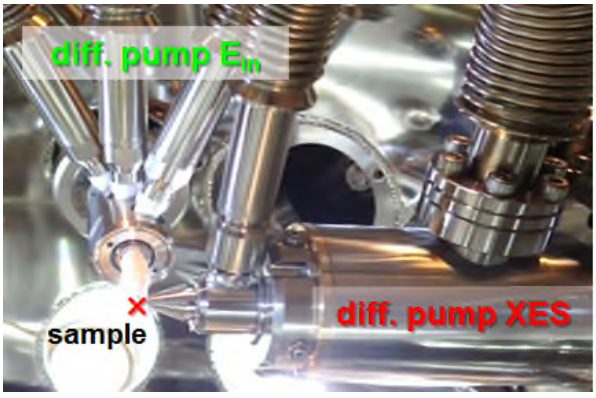

Fig. 1 Differential pumping system for ambient pressure soft X-ray RIXS experiments

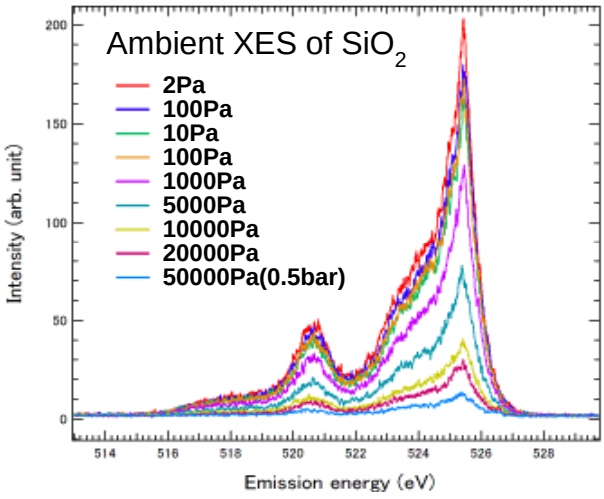

Fig. 2 Gas pressure dependence O K-edge RIXS spectra of SiO_2 from 2Pa to quasi-ambient pressure (0.5bar).

Figure 3 shows the spectrometer rotation system developed in our laboratory and just installed in our endstation. The three-axis rotation chamber for automatic and continuous rotation of the soft X-ray emission port along the horizontal axis was originally designed and applied for patent, which enables ±45 degrees continuous rotation of the RIXS spectrometer from the horizontal perpendicular direction to the incident beam. The ultra-precise position control system on a distortion- and vibration-free

rigid base plate enables us not to lose the focusing of a RIXS spectrum upon the spectrometer rotation.

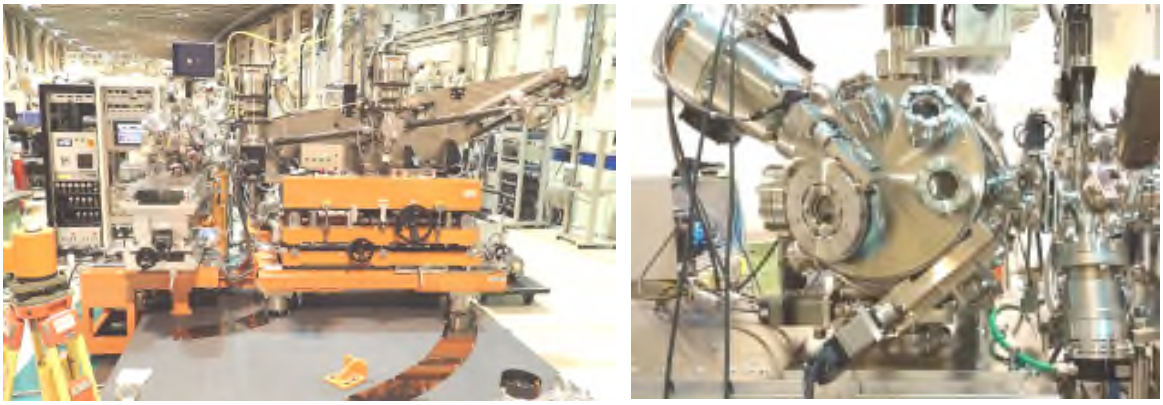

Fig. 3 Ultra-precise rotation system for angle resolved soft X-ray RIXS experiments; (a) full image of the spectrometer system (b) three-axis rotation chamber.

Low energy property of one-dimensional metallic surface states of Pt-induced atomic nanowires on Ge(001)

Koichiro Yaji and Fumio Komori
Institute for Solid State Physics, The University of Tokyo

One-dimensional (1D) electronic systems are well known as sources of intriguing physical phenomena such as a Tomonaga-Luttinger liquid (TLL) and Peierls-type metal-insulator transition. Besides, the surface bands split into two due to the Rashba effect if the 1D systems are including heavy element atoms. Platinum-induced atomic nanowires formed on a Ge(001) surface (Pt/Ge(001) NWs) are one of the suitable systems to study such peculiar phenomena of 1D electrons. The defect-less Pt/Ge(001) NWs was firstly observed by Gürlu *et al*. with scanning tunneling microscopy [1]. After that, Houselt *et al*. reported that the surface of Pt/Ge(001) NWs undergoes a structural phase transition at 80 K, where the high-temperature (HT) (low-temperature (LT)) phase exhibits a $p(4\times2)$ ($p(4\times4)$) periodicity [2]. Recently, we experimentally proposed the atomic configuration of Pt/Ge(001) NWs by means of reflection high-energy positron diffraction [3]. Detailed electronic band structures of Pt/Ge(001) NWs studied by angle-resolved photoelectron spectroscopy (ARPES) were reported in our previous paper [4], in which we identified two metallic bands derived from Pt/Ge(001) NWs (Fig. 1). One of the metallic bands (S_1) exhibits straight Fermi lines in the k_x–k_y space, indicating that electrons in this band behave as an ideal one-dimensional metal. Another metallic band (S_2) is a quasi-one-dimensional state because the band exhibits large two-dimensional undulation. Nevertheless, we have found no gap opening of the quasi-1D metallic bands at the Fermi level in the LT phase.

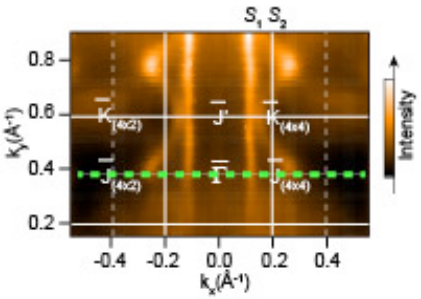

Fig. 1 Constant energy ARPES map at the Fermi level of Pt/Ge(001) NWs. Thin solid and dashed lines denote the boundaries of the SBZs of $p(4\times4)$ and $p(4\times2)$, respectively [4].

In the present study, we performed high-resolution ARPES with a vacuum ultraviolet laser light (laser-ARPES) to obtain precise information about both spin splitting and deviation from Fermi liquid behavior for the metallic bands.

The experiments were performed with the LOBSTER machine at Laser and Synchrotron Research Laboratory, the Institute for Solid State Physics [5]. The sample was *in situ* prepared in a molecular beam epitaxy chamber connected to an analysis chamber. We used a vicinal *n*-type Ge(001) substrate, which was tilted toward the [110] direction by 2°. A clean Ge(001) surface was prepared by several cycles of 0.5 keV Ar^+ ion bombardment at 670 K and annealing up to 900 K for a minute. Then, platinum was deposited onto the clean Ge(001) surface from a Pt wire heated by electron bombardment. The amount of deposited Pt was adjusted by checking the sharpness of low energy electron diffraction spots. In the laser-ARPES measurements, photoelectrons were excited by 6.994-eV photons and were analyzed with a ScientaOmicron DA30-L analyzer. The energy resolution of the laser-ARPES instruments was set to 2 meV. In the present study, we used linear-horizontal photon polarization, of which the electric-field vector is parallel to a light incident plane and a (110) plane of the Ge(001) substrate.

Figure 2(a) exhibits a laser-ARPES intensity image along $\bar{\Gamma}\bar{J}$ at 15 K [6]. In the upper panel of Fig. 2(a), an MDC at the binding energy of 5 meV is displayed. We clearly observed two metallic bands, S_1 and S_2. However, we found no splitting for both S_1 and S_2 even with the 2-meV energy resolution.

Next, we examined the density of states (DOS) analysis of the bands. Figure 2(b) displays energy distribution curves (EDCs) of S_1 and S_2, where the photoelectron intensities surrounded by rectangles shown in Fig. 2(a) were integrated to obtain the EDCs. We can recognize that a line shape of the EDC of S_1 is quite similar to that of S_2. In addition, we found that the photoelectron intensities from the S_1 and S_2 bands are slightly suppressed at the Fermi level and slopes of the EDCs around the Fermi level are gentle compared with that from the Au film.

The TLL scenario for S_2 is obviously ruled out because of the two-dimensional interaction. Thus, we suggest that the suppression of DOS for the S_2 band is attributed to the weak localization due to structural disorders on the surface. In contrast to the S_2 band, the S_1 band exhibits an ideal one-dimensional metallic property. Thus, we can consider two scenarios to explain the suppression of DOS of the S_1 band at the Fermi level. One of the scenarios is weak localization of the metallic electrons arising from the disorder, as seen in the S_2 band. The other scenario is a TLL picture. We analyzed the observed DOS of the S_1 band with a TLL spectral function considering the finite temperature [7]. From the fitting, we obtained an exponent α = 0.25. This exponent value is much smaller than that found in other TLL systems, such as carbon nanotubes, a lithium purple bronze and Bi/InSb(001). This indicates that electron-electron interaction of the S_1 band is rather weak compared with the other systems in the TLL scenario.

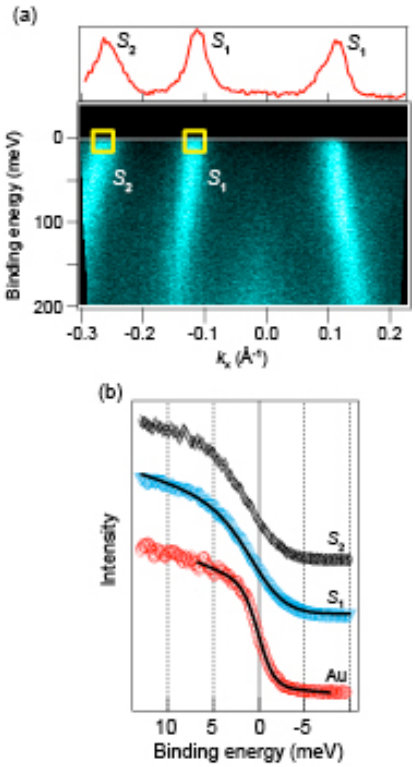

Fig. 2 (a) (*Upper panel*) The momentum distribution curve at the binding energy of 5 meV. (*lower panel*) ARPES intensity image recorded along a bold dashed line shown in Fig. 1. (b) (*Top*) The integrated EDC of S_2. (*Middle*) The integrated EDC of S_1. The solid curve represents a fitting result with the TLL spectral function considering the finite temperature. (*Bottom*) The Fermi edge taken from a Au film. The solid curve represents a fitting result with the Fermi-Dirac distribution function and polynomial background [6].

References

[1] O. Gürlu, O. A. O. Adam, H. J. W. Zandvliet and B. Poelsema, Appl. Phys. Lett. **83**, 4610 (2003).

[2] A. van Houselt, T. Gnielka, J. M. J. Aan de Brugh, N. Oncel, D. Kockmann, R. Heid, K. P. Bohnen, B. Poelsema, and H. J. W. Zandvliet, Surf. Sci. **602**, 1731 (2008).

[3] I. Mochizuki, Y. Fukaya, A. Kawasuso, K. Yaji, A. Harasawa, I. Matsuda, K. Wada and T. Hyodo, Phys. Rev. B **85**, 245438 (2012).

[4] K. Yaji, I. Mochizuki, S. Kim, Y. Takeichi, A. Harasawa, Y. Ohtsubo, P. Le Fèvre, F. Bertran, A. Taleb-Ibrahimi, A. Kakizaki and F. Komori, Phys. Rev. B **87**, 241413(R) (2013).

[5] K. Yaji, A. Harasawa, K. Kuroda, S. Toyohisa, M. Nakayama, Y. Ishida, A. Fukushima, S. Watanabe, C.-T Chen, F. Komori and S. Shin, Rev. Sci. Instrum. **87**, 053111 (2016).

[6] K. Yaji, S. Kim, I. Mochizuki, Y. Takeichi, Y. Ohtsubo, P. Le Fèvre, F. Bertran, A. Taleb-Ibrahimi, S. Shin and F. Komori, J. Phys.: Condens. Matter 28, 284001 (2016).

[7] K. Schönhammer and V. Meden, J. Electron Spectrosc. Relat. Phenom. **62**, 225 (1993).

SPIN-POLARIZED SURFACE ELECTRONS IN THE NOVEL SUPERCONDUCTOR Sr_2RuO_4 REVEALED BY LASER SPIN- AND ANGLE-RESOLVED PHOTOEMISSION SPECTROSCOPY

K. Kuroda[1], S. Akebi[1], M. Nakayama[1], K. Yaji[1], H. Taniguchi[2], Y. Maeno[2], S. Nakatsuji[1], T. Kondo[1]

[1]*The Institute for Solid State Physics, The University of Tokyo*

[2]*Deparatment of Physics, Kyoto University*

Introduction:

Since the discovery of superconductivity in Sr_2RuO_4, many theoretical and experimental efforts have been paid for examining spin-triplet chiral *p*-wave superconductivity [1-3]. However, some recent experiments have not supported this, in which spin-triplet superconductivity alone was insufficient to explain the experimental facts [4, 5]. This contradiction perhaps comes from the inclusion of low-energy fine-electronic structure and its wavefunction character due to spin-orbit coupling (SOC). In the presence of SOC, the quantum states with different orbitals and spins are generally mixed and the eigenstate wavefunction is strongly modified. In particular, it can be easily imagined that SOC possibly plays a fundamental role beyond simple models for Cooper pairing mechanism, since the energy scale of its SOC of nearly 100 meV is much larger than the scale of T_c ~0.2 meV. Moreover, similar to surface states on noble metals with strong SOC, in concert with an inversion-symmetry breaking at the surfaces, SOC raises the possibility that spin-polarized surface states, which can exist on the (001) cleaved surface. If it is realized, the chiral superconductivity topological edge states might be detected below T_c on the side surfaces [6]. Thus, it is an important key for understanding mechanism of superconductivity and topological characters in Sr_2RuO_4 to investigate roles of SOC in its electronic structure and wavefunction character. In this report, we have focused on the surface state in Sr_2RuO_4 and directly investigate the SOC state by using laser spin- and angle-resolved photoemission spectroscopy (laser-SARPES).

Experimental:

Laser-SARPES experiments were performed at newly home-built laser-SARPES machine at ISSP with high-flux 6.994-eV laser light [8]. The laser-SARPES machine is based on two high efficient VLEED spin-polarimeters and the hemispherical analyzer with photoelectron deflector function (ScientaOmicron DA30L). This spectrometer can resolve spin polarization components of photoelectrons in three-dimension for in-plane ($P_{x,y}$) and out-of-plane (P_z) orientation. The clean surface of Sr_2RuO_4 was *in situ* cleaved at below 10 K. During the measurement, the sample temperature was kept below 20 K, and instrumental energy and angular resolutions were set below 20 meV and 0.7°, respectively. All data was taken before sample degradation within 24 hours. Note that our laser photon energy is only sensitive to the surface states and thus the surface state can be selectively measured in our laser-SARPES experiments.

Results:

We start with a brief explanation for overall shape of Fermi surface obtained by our laser photon energy as shown in Fig. 1(a). The three-bands, α-band, γ-band and β-band, form the

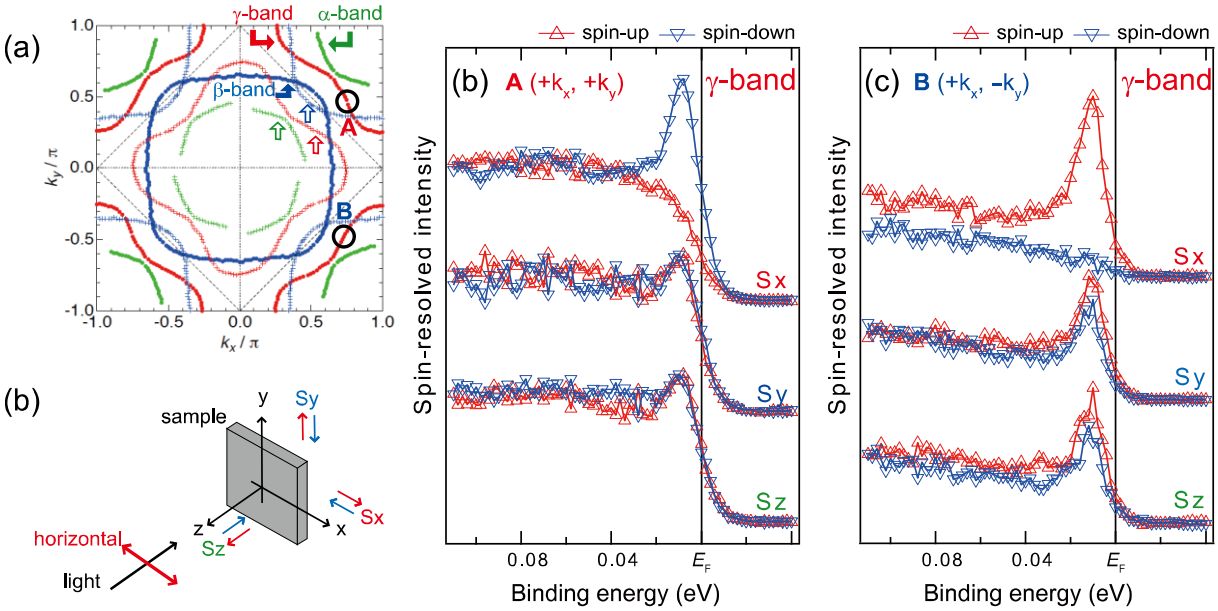

Fig. 1: (a) Shape of the Fermi surfaces for (001) cleaved surface of Sr_2RuO_4. Our laser photon energy enables us to selectively detect only the surface signals. The laser-SARPES experiments were done at **A** and **B**, corresponding to k_F of γ-bands. These two $k_{\parallel}$ points are symmetric with respect to the mirror plane (k_y=0 Å^{-1} plane). (b) The experimental configuration for **A** and **B,** and the definition of the spin orientations. (c) and (d) The spin-resolved energy-distribution curves at **A** and **B**, respectively.

Fermi surface indicated by closed arrows. Furthermore, due to the presence of strong surface relaxation [7, 8], these-three bands are folded denoted by opened arrows, and thus the surface states are strongly modified by not only SOC but also surface crystal potential, that is, inversion symmetry breaking. In this work we performed laser-SARPES at two symmetric $k_{\parallel}$ (**A** and **B**) as indicated by open circles, corresponding to γ-band near the Fermi level. We should note that the SARPES geometry for these two $k_{\parallel}$ is very simple: the laser electric field is applied normal to the surface, which is therefore sensitively to excite the in-plane orbital of the wavefunction. Figure 1(b) and (c) represent 3D-SARPES results at **A** and **B**, respectively [see Fig. 1(a)]. Red (blue) marks show the spin-up (spin-down) state for each axis. We observe clear spin-polarization at both $k_{\parallel}$ only along *x*-axis. Observed spin polarizations is found to be extremely large ~70 %. Importantly its orientations are symmetric: it aligns along +x direction at **A** but it turns to be –*x* at **B**. This symmetric spin-polarization indicates that the γ-band is intrinsically highly spin-polarized. Thus, we conclude that the SOC plays a role in the wavefucntion of Sr_2RuO_4 and moreover the surface state are highly spin-polarized due to the inversion-symmetry breaking. We stress that the modification of the wavefunction must be considered in the model for understanding Cooper paring mechanism in Sr_2RuO_4.

References:

[1] K. Ishida *et al*., Nature **396**, 658 (1998).
[2] T. M. Riseman *et al*., Nature **396**, 242 (1998).
[3] K. D. Nelson *et al*., Science **306**, 1151 (2004).
[4] S. Kittaka *et al*., Phys. Rev. B **80**, 174514 (2009).
[5] S. Yonezawa *et al*., Phys. Rev. Lett. **110**, 077003 (2013).
[6] S. Kashiwaya *et al*., Phys. Rev. Lett. **107**, 077003 (2011).
[7] K. M. Shen *et al*., Phys. Rev. B **64**, 180502 (2001).
[8] R. Matzdorf *et al*., Science **289**, 746 (2000).

LASER SPIN-AND ANGLE-RESOLVED PHOTOEMISSION STUDY ON SPIN-ORBITAL ENTANGLED SURFACE STATES OF TOPOLOGICAL INSULATORS

K. Kuroda, K. Yaji, A. Harasawa, M. Nakayama, F. Komori, T. Kondo
The Institute for Solid State Physics, The University of Tokyo

Introduction:

A central subject in the research for spintronic application is realization of functional capabilities to generate highly spin-polarized electrons and control its spin degree of freedom. As a promising spintronic material, a highly spin-polarized topological surface states (TSS) in three-dimensional topological insulators (TIs) has grabbed particular attentions. The TSS forms Dirac-cone-like energy dispersion and exhibits chiral spin texture in momentum space due to the strong spin-orbit coupling (SOC) [1]. The peculiar spin texture protects the TSS electron from electron backscattering, which makes the TSS robust against perturbations. The TSS therefore can be useful as a novel spin generator and conductor. Here, the TSS faces a new challenge for optical control over its spin properties. In addition to the chiral spin texture, it was proposed that the relativistic SOC plays an important role to blend quantum states with different spin and orbitals, which gives rise to a *"spin-orbital texture"* in TSSs as shown in Figure 1(A) [2]. Since electric field of light directly couples with the orbitals, through the entanglement of the spin and orbital parts of the wavefunction, it may enable us to optically manipulate the spin degree of freedom.

In this report, by a combination of SARPES technique with three-dimensional (3D) spin-resolution and polarization-variable vacuum-ultraviolet (VUV) laser, we demonstrate the spin-orbital texture of TSS in Bi_2Se_3. We show that symmetric experimental configurations for *p*- or *s*-polarization set-up selectively excite either spin-up or spin-down state from the spin-orbital textures, which is available for novel optspintronic devices.

Experimental:

Laser-SARPES was performed at newly home-built laser-SARPES machine at ISSP with high-flux 6.994-eV laser light [3]. The laser-SARPES machine is based on two high efficient VLEED spin-polarimeters and the hemispherical analyzer with photoelectron deflector function (ScientaOmicron DA30L). This spectrometer can resolve spin polarization components of photoelectrons for in-plane ($P_{x,y}$) and out-of-plane (P_z) orientation. These spin polarized photoelectrons are excited by *p*- or *s*-polarized light as shown in Fig. 1(B) and (C). During the measurement, the sample temperature was kept below 20 K, and instrumental energy and angular resolutions were set below 20 meV and 0.7°, respectively.

Results:

Figure 1(D) represents standard ARPES intensity map for Bi_2Se_3 along the Γ-M high symmetry line of the surface Brillouin zone. The data well resolves the sharp TSS with the Dirac-cone-like energy dispersion and the bulk conduction band at the center of the surface state. Figure 1 (E) and (F) show the three-dimensionally spin-resolved energy distribution curves (EDCs) and the corresponding spin polarization curves obtained at $(k_x, k_y) = (-k_F, 0)$ [dashed line in Fig. 1(D)] by using *p*- and *s*-polarization geometry, respectively. For the *y*-spin polarization (P_y), our data clearly shows nearly ±100% reversal property of photoelectron spin polarization with switching the light electric field between. As a consequence of the full polarization of P_y, the perpendicular components, P_x and P_z, are

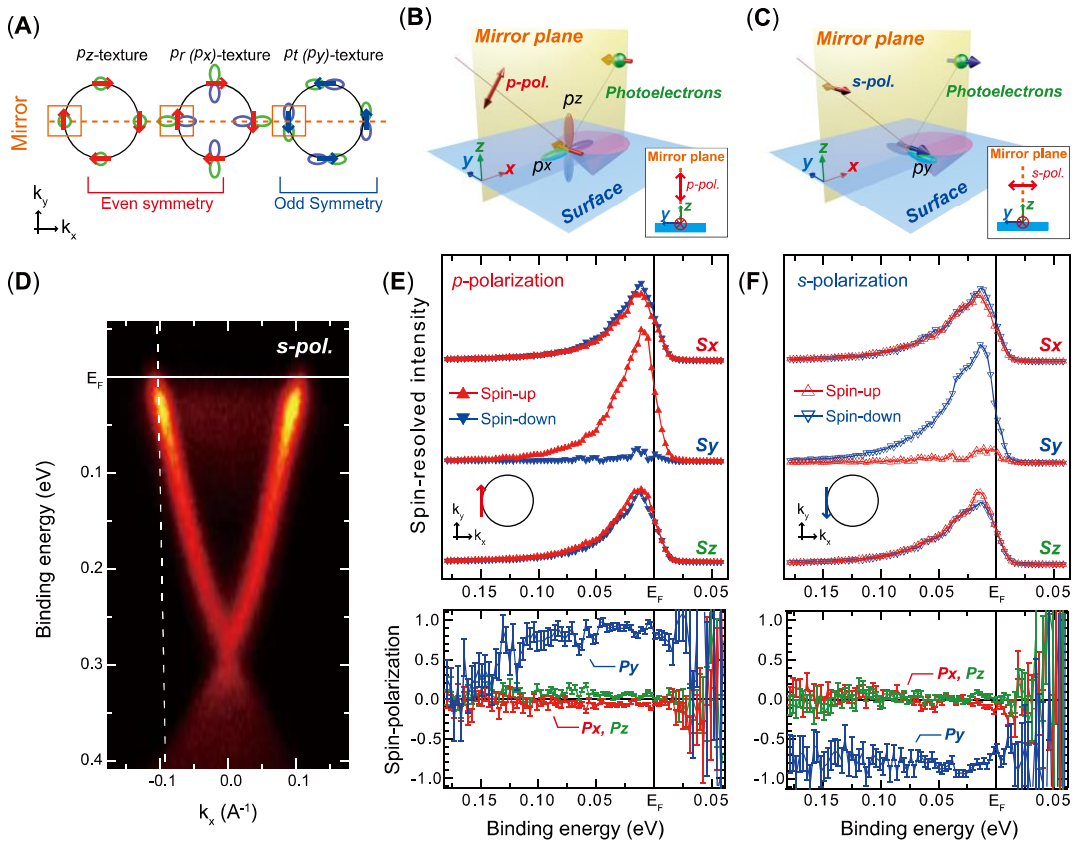

Fig. 1: (A) The schematics for the spin-orbital texture for the upper topological surface state [2]. (left, middle) p_z and the tangential orbital texture (p_t) with the right-handed helical spin texture and (right) the radial orbital texture (p_r) with the different spin texture. (B), (C) The experimental configuration for *p*- and *s*-polarization. The light incidence plane and the detection plane match the mirror plane of the crystal. The *s*- (*p*-) polarization excites *odd* (*even*) parity orbitals with respect to the mirror plane [the dashed line in Fig. 1(A)], which is corresponding to p_y (p_z and p_x) like orbitals. (D) ARPES intensity map along the Γ-M symmetry line. (E), (F) Three-dimensional spin-resolved photoemission intensity and the corresponding spin polarization as a function of binding energy obtained by *p*- and *s*-polarizations, at fixed emission angle corresponding to the dashed line-cut in (D). The observed spin orientations are shown in the insets.

negligibly small for the both linear polarizations. These observed fully spin-polarized photoelectrons can be directly imagined from the spin-orbital textures as shown in Fig. 1 (A) and general dipole selection rule for *even-odd* parity orbitals. In the textures, *p*-polarized light selectively excites *even* components with p_z- and p_x-like orbitals, which is fully spin polarized along *y* at $-k_x$ location [left and middle textures in Fig. 1(a)]. On the other hand, the photoelectrons are emitted only from *odd* one of p_y-like orbital coupled with the opposite spin orientation by s-polarized light [right textures in Fig. 1(a)].

References:

[1] M. Z. Hasan, C. L. Kane, Rev. Mod. Phys. **82**, 3045 (2010).
[2] H. Zhang, C.-X. Liu, S.-C. Zhang, Phys. Rev. Lett. **111**, 066801 (2013).
[3] K. Yaji *et al*., Rev. Sci. Instrum., **87**, 053111 (2016).

TESTING THE SURFACE PHOTOELECTRIC EFFECT

Y. Ishida, K. Yaji, S. Shin
The Institute for Solid State Physics, The University of Tokyo

A long-wavelength approximation is often assumed *a priori* when the interaction between light and matter is concerned. The assumption, however, may be strongly invalidated in the surface region at the atomic scale, particularly when the photon energy is low [1]. Here, we test its validity in the photoelectric effect.

When the long-wavelength approximation is valid, the electrons subjected to the photon field $\boldsymbol{A}$ cannot sense the direction of the light propagation. The validity can thus be tested by investigating whether or not the angular distribution of photoelectrons depends on the propagation vector of the light. Figure 1(a) shows the setup for the test. Here, the 7-eV light is *s*-polarized, and the photoelectrons are collected by Scienta-Omicron analyser [2]. In this configuration, it is only the propagation vector that breaks the mirror symmetry of the setup with respect to the plane spanned by the *s*-polarization vector and surface normal of the sample. The photoelectron distribution thus becomes asymmetric (symmetric) with respect to the geometrical mirror plane when the photoelectric effect is susceptible (unsusceptible) to the propagation vector. Here, the sample should not break the mirror symmetry: To fulfil this condition, we chose highly-oriented Bi microcrystals grown on a highly-oriented pyro-graphite for the sample [3]. The microcrystals are randomly oriented in plane with their 111 face oriented normal to surface, so that the effect of the crystal symmetry is averaged out in the azimuth.

Figure 1(b) shows the angular distribution of photoelectrons at the binding energy E_B = 60 meV; that is, the distribution is of the photoelectrons emitted from the surface states on Bi(111). A Debye-ring-like distribution is observed due to the random in-plane orientation of the microcrystals. Clearly, the distribution is asymmetric about the geometrical mirror plane, $\Theta_X = 0$. The result shows that the photoemission from the surface-localized electrons depends on the propagation vector of the *s*-polarized light; thus the breakdown of the approximation.

Based on the jellium model, the breakdown occurs only for *p*-polarized component of $\boldsymbol{A}$ [1]. The present result thus calls for a description beyond. We note that the three-slab model often used in the field of surface nonlinear optics can qualitatively explicate the phenomena.

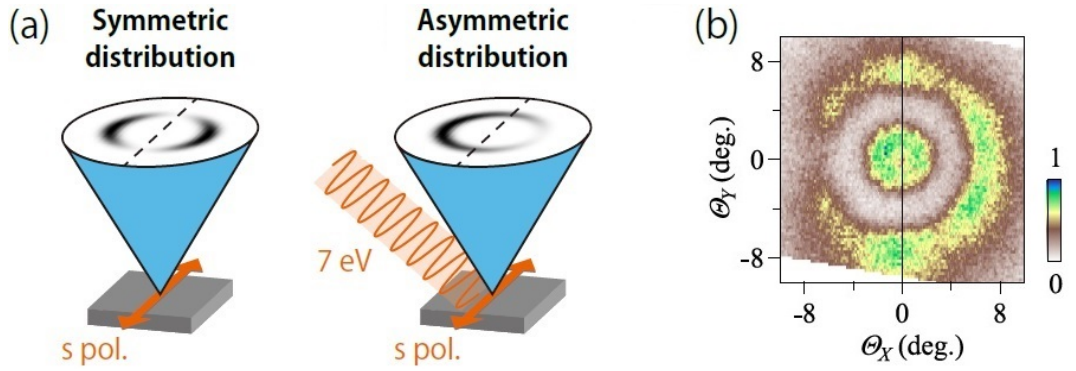

Fig. 1: Testing the surface photoelectric effect. (a) Experimental geometry. Photoelectron distribution becomes asymmetric (symmetric) when the photoelectric effect is susceptible (unsuceptible) to the propagation vector of light. (b) Distribution of photoelectrons emitted from highly-oriented Bi(111).

REFERENCES

[1] H. J. Levinson, E. W. Plummer, and P. J. Feibelman, Phys. Rev. Lett. **43**, 952 (1979).
[2] K. Yaji *et al.*, Rev. Sci. Instrum. **87**, 053111 (2016).
[3] Y. Ishida *et al.*, Submitted.

SPIN POLARIZATION OF 1D SURFACE STATE ON BI/INSB(001)

J. Kishi[1], Y. Ohtsubo[1,2], A. Harasawa[3], K. Yaji[3], F. Komori[3], S. Shin[3], S. Kimura[1,2]
[1]*Department of Physics, Graduate School of Science, Osaka University*
[2]*Graduate School of Frontier Biosciences, Osaka University*
[3]*Insutitute for Solid State Physics, The University of Tokyo*

A spin-polarized electronic state is one of the key element for future spintronic devices. The spin-polarized states are not only the source of spin-polarized electric current but also applicable for ballistic electron transport thanks to the restricted backscattering due to the spin-dependent scattering process. For this purpose, surface states on topological insulators [1] and related materials containing heavy elements with strong spin-orbit interaction (SOI) [2-7] are attracting much attention in recent days. The surface states of Bi are one of the typical examples and have been studied extensively for this decade: surface states on Bi(111) single crystal [3], Bi(111) ultrathin films [4, 5].

In this work, we fabricated Bi ultrathin film on the InSb(001)-*c*(8×2) substrate and determined the surface electronic structure and its spin polarization by the spin- and angle-resolved photoelectron spectroscopy using a laser (laser-SARPES) at the Institute for Solid State Physics (ISSP). The electronic and atomic structures of Bi ultrathin films on InSb(001) showed obvious one-dimensional (1D) character, which is a clear difference from the well-known case grown on Si(111) [4, 5].

Figure 1(a) shows the low-energy electron diffraction (LEED) pattern of the Bi/InSb(001) film. The pattern is streaky along the vertical direction, possibly due to the variety of the surface periodicity along this direction. In contrast, the width of the pattern along the lateral direction is sharp, indicating well-defined surface order along this direction. Such 1D surface atomic structure would be due to an anisotropic surface atomic structure of the clean surface of InSb(001)-*c*(8×2) substrates.

Figure 1(b) shows the spin-integrated surface band dispersion observed by the laser-SARPES setup. The wave vector *k* in Fig. 1(b) is parallel to the horizontal direction in Fig. 1(a). Along this direction, the observed band showed clear Λ-shape dispersion. Since such dispersion is absent in the substrate band structure, it is from the 1D Bi film. Actually, the Λ band was less dispersive along the direction parallel to the vertical axis in Fig. 1(a). Moreover, the band structure can be fitted with a linear line well. And then, the band velocity along the *k* direction can be estimated to be ~5.0×10^5 (m/s), which is in the same order of magnitude as that of the Dirac point in graphene, suggesting possible applications to future high speed electron transport via this surface state. Figure 1(c) shows the spin-resolved MDC at 0.1 eV below the Fermi level (E_F). The up (down) spin represents the spin polarization along the direction parallel (anti-parallel) to the vertical direction in Fig. 1 (a): in other words, the direction perpendicular to the wave vector and the surface normal. The MDCs in Fig. 1 (c) indicate that the spin polarization inverts with respect to the normal emission. These spin-polarized characters of surface states are what is expected for topological surface states and/or Rashba-type spin-split surface bands.

Different from ordinal spin-polarized Dirac cones on topological insulators, the Λ-shape surface state has finite bandgap around E_F. Figure 1 (d) shows the ARPES energy distribution curves at the room temperature along *k* divided by a Fermi-Dirac distribution function convoluted with the instrumental resolution. The bottom of unoccupied state is just above the top of occupied state which has Λ shape, and the direct energy gap between them can be estimated to be ~150 meV. It means that electrons at room temperature unlikely jump over this energy gap due to thermal excitation.

In summary, we observed pseudo one dimensional surface electronic states on Bi ultrathin film grown on InSb(001) by laser-SARPES, which have attractive properties: high electron mobility from steep dispersion, spin polarization possibly realizing backscattering-free transport, and the direct band gap larger than thermal Fermi-level broadening at RT. These properties will open the way to future application of this material for spintronic devices.

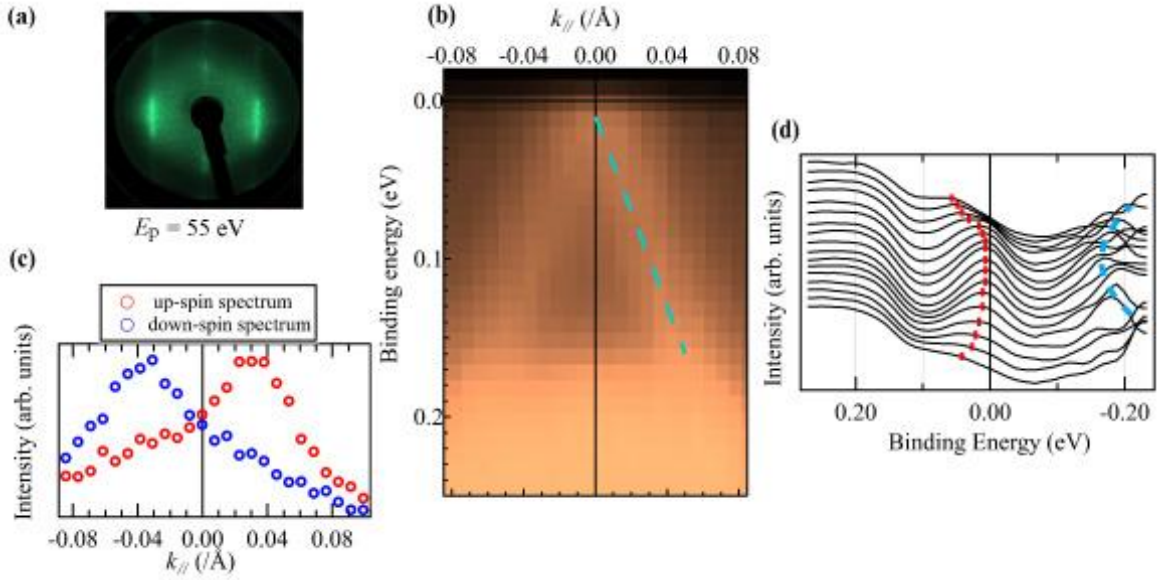

Figure 1: (a) A Low Energy Electron Diffraction (LEED) pattern of the Bi/InSb(001) surface at room temperature (RT). (b) ARPES intensity map along k parallel to the horizontal direction in (a). A dashed line (blue) is guide to the eye for the surface band. (c) Spin-resolved momentum distribution curves taken at 0.1 eV. (d) ARPES energy distribution curves along k, divided by the Fermi-Dirac distribution function at RT convoluted with the instrumental resolution.

REFERENCES

[1] M. Z. Hasan and C. L. Kane, Rev. Mod. Phys. **82**, 3045 (2010).
[2] T. Okuda and A. Kimura, JPSJ **82**, 021002 (2013)
[3] C. R. Ast *et al.*, Phys. Rev. Lett. **98**, 186807(2007)
[4] T. Hirahara *et al.*, Phys. Rev. B **76**, 153305(2007)
[5] A. Takayama *et al.*, Phys. Rev. Lett. **106**, 166401(2011)
[6] J. W. Wells *et al.*, Phys. Rev. Lett. **102**, 096802(2009)
[7] M. Bianchi *et al.*, Phys. Rev. B **91**, 165307 (2015)

Staff

Director: SHIN Shik

KOMORI Fumio

MATSUDA Iwao, Associate Professor
HARADA Yoshihisa, Associate Professor
WADATI Hiroki, Associate Professor
FUJISAWA Masami, Research Associate
YAMAMOTO Susumu, Research Associate
YAJI Koichiro, Research Associate
MIYAWAKI Jun, Research Associate
HIRATA Yasuyuki, Research Associate
FUKUSHIMA Akiko, Technical Associate
SHIBUYA Takashi, Technical Associate
HARASAWA Ayumi, Technical Associate
KUDO Hirofumi, Technical Associate

Technical Assistant: KOSEGAWA Yuka
ARAKI Mihoko

Secretary: AIHARA Yumiko
HARADA Misa(~2015.5, 2015.12~)
KANEKO Yoshie
MITSUDA Emi(~2016.2)
HAYASHI Akiko(~2015.9)
YOSHIZAWA Motoko(2015.5~)
TSUTSUMI Yumiko(2015.5~)
IKEDA Kuniko(2015.11~)

Graduate Student: KIUCHI Hisao
YAMAMOTO Shingo
KUBOTA Yuya
RO-Ya-Liu
SOMEYA Takashi

ITOH Suguru
TAKEUCHI Kaori
ITAMOTO Haruki
INOUE Takanobu
YAMAMOTO Kohei
WANG Hao

Contract Researcher: NIWA Hideharu(~ 2015.7)
TAKUBO Kou
CUI Yitao
FENG Baojie

Publication List(2015)

---Harima---

Characterization of nitrogen species incorporated into graphite using low energy nitrogen ion sputtering

Kiuchi, Takahiro Kondo, Masataka Sakurai, Donghui Guo, Junji Nakamura, Hideharu Niwa, Jun Miyawaki, Maki Kawai, Masaharu Oshima, and Yoshihisa Harada,Phys. Chem. *Chem. Lett.**18**,458-465 (2016)*

Electron-phonon coupling in the bulk of anatase TiO_2 measured by RIXS

S. Moser, S. Fatale, P. Krüger, H. Berger, P. Bugnon, A. Magrez, H. Niwa, J. Miyawaki, Y. Harada, and M. Grioni, *Phys. Rev. Lett.**115**.096404 (2015)*

Ultrafast spin-switching of a ferrimagnetic alloy at room temperature traced by resonant magneto-optical Kerr effect using a seeded free electron laser

Sh. Yamamoto, M. Taguchi, T. Someya, Y. Kubota, S. Ito, H. Wadati, M. Fujisawa, F. Capotondi, E. Pedersoli, M. Manfredda, F. Casolari, Maya Kiskinova, J. Fujii, P. Moras, T. Nakamura, T. Kato, T. Higashide, S. Iwata, S. Yamamoto, S. Shin, and I. Matsuda, *Rev. Sci. Instrum. **86**, 083901 (2015)*.

Perspectives of in situ/operando resonant inelastic X-ray scattering incatalytic energy materials science

Yi-Sheng Liu, Per-Anders Glans, Cheng-Hao Chuang, Mukes Kapilashrami, Jinghua Guo, *Journal of Electron Spectroscopy and Related Phenomena **200**, 282-292 (2015).*

Anisotropic effective mass approach for multiple subband structures at wide-gap semiconductor surfaces: Application to accumulation layers of $SrTiO_3$ and ZnO

R. Yukawa, K. Ozawa, S. Yamamoto, R.-Y. Liu, and I. Matsuda, *Surf. Sci. **641**, 224-230 (2015).*

Chemical potential shift in organic field-effect transistors identified by soft X-ray operando nano-spectroscopy

Naoka Nagamura, Yuta Kitada, Junto Tsurumi, Hiroyuki Matsui, Koji Horiba, Itaru Honma, Jun Takeya and Masaharu Oshima, *Appl. Phys. Lett., **106**, 251604 (2015).*

Highly Brilliant Synchrotron Radiation Operando Spectromicroscopy to Bridge a Gap between Material Electronic Properties and Device Performances of 2D Atomic Layers

吹留　博一,　*表面科学, **36(6)**, 303-308 (2015).*

Multi-phonon excitations in Fe 2p RIXS on Mg_2FeH_6

K. Kurita, D. Sekiba, I. Harayama, K. Chito, Y. Harada, H. Kiuchi, M. Oshima, S. Takagi, M. Matsuo, R. Sato, K. Aoki, S. Orimo, J. *Phys. Soc. Jpn. **84**, 043201 (2015)*.

X-ray spectroscopic study of $BaFeO_3$ thin films: An Fe^{4+} ferromagnetic insulator

T. Tsuyama, T. Matsuda, S. Chakraverty, J. Okamoto, E. Ikenaga, A. Tanaka, T. Mizokawa, H. Y. Hwang, Y. Tokura, and H. Wadati, *Phys. Rev. **B 91**,115101 (2015)*..

X-ray Emission Spectroscopy of Bulk Liquid Water in "No-man's Land

J. Sellberg, T. McQueen, H. Laksmono, S. Schreck, M Beye, D. DePonte, B. O'Kennedy, D. Nordlund, R. Sierra, D. Schlesinger, T. Tokushima, S. Eckert, V. Segtnan, H. Ogasawara, K. Kubicek, S. Techert, U. Bergmann, G. Dakovski, W. Schlotter, Y. Harada, I. Zhovtobriukh, M. Bogan, P. Wernet, A. Föhlisch, L. Pettersson and A. Nilsson, J. *Chem. Phys.* ***142****, 044505 (2015).*

A close look at dose: Towards L-edge XAS spectral uniformity, dose quantification and prediction of metal ion photoreduction

M.M. van Schooneveld and S. DeBeer, J. Electron Spectrosc. Relat. *Phenom.* ***198****, 31 (2015).*

Operando soft x-ray emission spectroscopy of $LiMn_2O_4$ thin film involving Li-ion extraction/insertion reaction

D. Asakura, E. Hosono, H. Niwa, H. Kiuchi, J. Miyawaki, Y. Nanba, M. Okubo, H. Matsuda, H.S. Zhou, M. Oshima, and Y. Harada, *Electrochem. Commun.* ***50****, 93 (2015).*

---E-labo---

Spin polarization and texture of the Fermi arcs in the Weyl Fermion semimetal TaAs

S.-Y.Xu, I.Belopolski, D.S.Sanchez, M.Neupane, G.Chang, K.Yaji, Z. Yuan, C. Zhang, K.Kuroda, G. Bian, C. Guo, H. Lu, Y. Feng, T.-R. Chang, N. Alidoust, H. Zheng, C.-C. Lee, S.-M. Huang, C.-H. Hsu, Horng-Tay Jeng, A. Bansil, A. Alexandradinata, T. Neupert, T. Kondo, S.Shin, H.Lin, S.Jia, M Z.Hasan *Phys. Rev. Lett.* ***116****, 096801 (2016)*